ORIGINAL PAPER

Spatial–temporal prediction model for land cover of the rural–urban continuum axis between Ar-Riyadh and Al-Kharj cities in KSA in the year of 2030 using the integration of CA–Markov model, GIS-MCA, and AHP

Ashraf Abdelkarim[1,2] ⬤ · **Haya M. Alogayell**[3] · **Ibtesam I. Alkadi**[3] · **Ismail Youssef**[4]

Abstract

The spatiotemporal analysis of land use/land cover change and monitoring, modeling, and forecasting the future of land uses are considered challenges facing planners and decision-makers in developing countries. These challenges are increased in neighborhood areas surrounding large cities, which are known as the "rural–urban continuum". These areas have become the preferred areas for resettlement for most urban residents. The objectives of the present study were to (1) monitor the land cover change in the rural–urban continuum axis between the Ar-Riyadh and Al-Kharj cities during the period 1988–2020, (2) simulate the future growth of land cover up to the year 2030 using the Cellular Automated Markov Model (CA-Markov), and (3) improve the ability of CA-Markov to predict the future by integrating multi-criteria analysis based on geographic information systems (GIS-MCA) and analytic hierarchy process (AHP) method. The results of the study revealed large changes in the land cover in the rural–urban continuum axis between the Ar-Riyadh and Al-Kharj cities. About 60 km^2 of agricultural land has been lost, with an average annual decrease of 2 km^2. The industrial and urban areas were increased with growth rate of 4%. There were five categories of spatial suitability, ranging between 32 and 86%, and 70% or higher is the recommended percentage for future land uses. The industrial use was the most likely land use in 2030, as it recorded an increase of 27.1 km^2 over the year 2020.

Keywords Spatiotemporal framework prediction · Urban sprawl · Land cover changes · Rural–urban continuum axis · Ar-Riyadh-Al-Kharj · CA-Markov · GIS-MCA · AHP · Future land cover

✉ Ashraf Abdelkarim
dr.ashrafgis2020@gmail.com

Haya M. Alogayell
hayaalogayell@gmail.com

Ibtesam I. Alkadi
Ebtesam.K@gmail.com

Ismail Youssef
youssefegyptgeo@gmail.com

1 Social Studies Department, College of Arts, King Faisal University, Al-Ahsa'a, 380, Riyadh, Saudi Arabia

2 Research Center, Ministry of Housing (Previously), Ar-Riyadh 84428, Saudi Arabia

3 Geography Department, College of Arts, Princess Nourah Bint Abdulrahman University, Ar-Riyadh 84428, Saudi Arabia

4 Department of Geography, Faculty of Art, Monofiya University, Shbeen El Koom 32511, Egypt

Introduction

The urban planning of land use in cities, major capitals, and neighborhood of urban communities constitutes crucial issue in the field of urban development. During the last decades, studying the land use/cover became a popular topic as it related to environmental, biological, and ecological processes (Foley et al. 2005; Mwangi et al. 2017; Behera et al. 2012). The most common and widespread land use/cover changes around the world are deforestation, agricultural expansion, and urbanization (Mubea et al. 2014; Hosonuma et al. 2012; Geist and Lambin 2001). Changes in land cover affect land use, climate change (Feddema et al. 2005), desertification (Turner 1994), and global environmental change (Mbiba and Huchzermeyer 2002). The urban planners and policymakers around the world have a growing interest to study the neighborhood of urban areas. The neighborhood of

urban areas known as the rural urban continuum has become the preferred areas for resettlement for most of the urban population as the rent is relatively affordable, to work in economic, commercial and agricultural activities (Simon et al. 2004); (Kombe 2005), and for the availability of main agricultural lands and their proximity to the city (Thuo 2010; Tajbakhsh et al. 2016; Mandere et al. 2010; Acheampong and Anokye 2013; Gibbs and Salmon 2015). Modeling and simulating the land use are important tools for urban planning, policy formulation, and assessing the impacts of land use change on the ecological environment (Foley et al. 2005; Geist and Lambin 2001). Cellular automata model is the most popular technique to model land use changes since the 1990s (Guan et al. 2011; White and Engelen 2000a, 1994; Santé et al. 2010; Li et al. 2017; Batty and Xie 1994; Wu 1998, 2002). Accurate simulations and predictions of urbanization and land use are essential in urban management and addressing trends and temporal-spatial distributions, The CA–Markov model has proved high efficiency in the modeling and simulating of urban growth and predicting future land uses. Simulation of land use with the CA–Markov model improves the understanding of the complex dynamic processes of land use change that cannot be achieved through conventional models (Pakawan and Saowanee 2019; Solomon et al. 2019; Taher et al. 2018; Rahel et al. 2018; Ahmadreza et al. 2016).

Cellular locally interacting Markov model or Cellular Automata is an integration of the cellular locally interacting model or Cellular Automata and Markov model, where the Markov model is a method of analyzing the current behavior of a particular variable for the purposes of predicting the future behavior of this particular variable. Markov chains are named after their discoverer Andrea Markov, the Russian scientist. Markov chains represent one of the "dynamic programming" tools, which are methods of operation researches used to support decision-making when the future status depends on the current status as a forecasting technique. The cellular locally interacting model or Cellular Automata is a mathematical software model that enables us to predict the future on the assumption that cells can take a finite number of states where each future state of the cell is related to its current state and the states of neighboring cells. The transformation from one state to another is governed by predefined rules that depend on the successive developments and the previous states of the cell and of neighboring cells.

In light of the outputs of Change Analysis application and Transition Potential Modeling, the model of Change Prediction analysis is run, where the future scenario of the change can be predicted at a future date.

Although CA-Markov is one of the most widely used models to predict land use changes, it has a great limitation as it is affected by human bias and does not accurately reflect potential nonlinear relationships between land use change

factors. To overcome this limitation, GIS and multi-criteria analysis (GIS-MCA) and AHP method were combined.

Malczewski (Malczewski 2006) defined GIS-based MCDA as a process that combines the preferences of the spatial data and the values law to generate information to be provided to decision-makers (Malczewski 1999; Chakhar and Mousseau 2008; Yatsalo et al. 2010; Reynolds and Hessburg 2014; Dell'Ovo et al. 2018; Janssen and Rietveld 1990; Carver 1991; Rinner and Heppleston 2006). GIS-based MCDA includes evaluating the spatial decision alternatives that were determined based on the parameters and preferences of decision-makers. Multi-criteria decision analysis (MCDA) is generally used to evaluate multiple parameters. The decision-making process mainly involves four stages: defining the problem, building the preferences of decision-makers, evaluating the alternatives, and determining the best of the alternatives (Simon 1977; Tzeng and Huang 2011). Integrating MCDA and GIS is a great contribution that usually yields very useful spatial alternatives to help decision-makers.

The main purpose of using MCA is to improve the ability of the CA-Markov cellular model to predict the future of land cover in 2030 using twelve criteria. The analytic hierarchy process (AHP) method that was developed by Saaty (Bossche et al. 2018) is one of the most important methods for analyzing the land suitability and providing the decision-makers and planners with the statistical analysis data before giving their final decision regarding the future changes in land uses (Lee and Yeh 2009; Pan and Pan 2012; Hasan et al. 2019; Araya et al. 2018). Integration of AHP and GIS was done for determining the importance of the used criteria and calculating their weights according to the importance with regard to the experts' opinions (Merlos et al. 2015; Baja et al. 2018; Huiping et al. 2019).

Several studies showed that the CA–Markov model is able to simulate and predict the spatial process of urban development and efficiently predict land use (Silva and Clarke 2002; Liu 2009; Oguz et al. 2007; Ding and Zhang 2007). CA-Markov can be combined with other techniques such as GIS-MCA and AHP (Webster and Wu 2001; White and Engelen 2000b; Abd El Karim and Mohsen 2020; Abdelkarim 2020; Abdelkarim et al. 2020) to model future land uses (Oguz et al. 2007; Saidi et al. 2017; Jin and Álvaro 2017).

The CA–Markov model has diverse advantages in simulating land uses (Parsa and Salehi 2016; He et al. 2017b; Xu et al. 2016) as it simulates complex land use patterns based on simple local transformational rules. CA–Markov model can be combined with GIS and remote sensing data to improve the capabilities of GIS to analyze complex, temporal, and spatial complex natural feature (He et al. 2008). Land use prediction models have been developed to focus on a set of multiple models with several natural, social, and economic factors based on GIS-MCA and AHP method which

makes the simulations of land use change more accurate (Liu et al. 2017).

This study aims to (1) monitor the land cover changes in the rural–urban continuum axis between the Ar-Riyadh and Al-Kharj cities during the period 1988–2020 using the supervised classification of Landsat satellite images acquired in years 1988, 2000 and 2013, and 2020; (2) predict and simulate the future land use growth in year 2030 using the CA–Markov model; (3) improve the CA–Markov model through integration with the GIS-MCA; and (AHP) to cover the factors of land use changes in the rural–urban continuum axis between the Ar-Riyadh and Al-Kharj cities.

The problem of this research was focused on studying the contradiction between the national urban strategy for land use in the Kingdom and the comprehensive plan for Al-Kharj governorate. On the other hand, the national urban strategy for land use in the Kingdom recommends the increased industrial, commercial, and agricultural activities in the study area to support the economic aspect of the central region in the Kingdom. The comprehensive plan for Al-Kharj governorate proposes that the land uses in the study area are recommended to be agricultural and free of any industrial activities. The study is also interested in examining the impacts of the rapid population growth in the cities of Ar-Riyadh and Al-Kharj as the population has doubled over the past 30 years, 5 times and 3.3 times for Ar-Riyadh and Al-Kharj, respectively. This population increase led the population to move towards the rural–urban continuum axis between the two cities resulted in the encroachments at the expense of agricultural lands. The results of the present study indicated that the agricultural lands lost about 60 km^2 of its total area during the past 30 years during the period 1988–2020, with an average annual decrease of 2 km^2 and the industrial areas increased at a growth rate of 4%. This imbalances increases and decreases have led to (1) an imbalance of the population component, (2) deterioration of the urban fabric, (3) lack and misdistribution of services, (4) penetration and control of industrial use at the expense of other uses, (5) increase in environmental changes, and (6) loss of the environmental and ecological balance of the characteristics of the study area. The acceleration of urbanization and industrialization affects the regional development of the urban–rural continuum axis between Ar-Riyadh and Al-Kharj, and achieving the balance between economic development and environmental protection became a major issue for planners and policymakers in Saudi Arabia.

Study area

The rural–urban continuum axis is located between the cities of Ar-Riyadh and Al-Kharj on the Ar-Riyadh-Al-Kharj highway with a length of 45 km and an average width of 4.5 km on both sides of the highway. The rural–urban continuum axis is located between the two latitude 24° 13′ 58.31″ and 24° 29′ 48.57″ in the north and between longitudes 46° 56′ 29.62″ to 47° 12′ 44.44″ in the east as seen in Fig. 1.

The continuum extends from the end of the industrial city in the south of Ar-Riyadh until the beginning of the borders of exit number seven in the north of the city of Al-Kharj. The rural–urban continuum axis includes about seven urban agglomerations, namely, from south to north: Al Bijadiyah, Ar Rufayi', Souther Hit, Al Aammaieh, Al ljamn, Dahl Hit, and Al Riya. The population of the urban rural continuum area is about 16,819 people (General Authority for Statistics, 2018). The urban rural continuum axis is characterized by the different land uses, which is dominated by industrial use, in addition to palm farms with the associated agricultural industries, recreational activities, camping areas, squares, and rest areas as shown in Fig. 2.

Study procedures and data processing

The study procedures and data processing are shown in Fig. 3 that included three main steps: firstly, monitoring changes in land use during 1988–2020; secondly, multi-criteria analysis based on geographic information systems and determination of weights using hierarchical analysis; and thirdly, using the Cellular Automata Markov model to predict land uses in 2030.

### Monitoring changes in land cover during 1988–2020:

The process of monitoring land cover changes for the rural–urban continuum between the cities of Ar-Riyadh and Al-Kharj during the period 1988–2020 is consisted of a set of stages that can be summarized as follows:

The first stage was downloading of four satellite images in 1988 and 2000 from the Landsat-TM and 2013 and 2020 from Landsat-OLI to monitor changes in land cover in the urban rural continuum axis between Ar-Riyadh and Al-Kharj during the period 1988–2020. Table 1 and Fig. 4 present details about the satellite images from 1988 to 2020.

The second stage: band combination
The stage of band combination is one of the necessary stages to show the satellite images in their natural or true colors and to choose the appropriate ranges for the three colored ranges RGB, in order for the feature to appear in their true earthly colors through Multi-

Fig. 1 Location of the rural–urban continuum axis between Ar-Riyadh and Al-Kharj from the Kingdom of Saudi Arabia in 2020. Source: **A** KSA official map, Geo Portal, General Commission of survey; **B** Atlas distribution maps of the primary results of the General Population and Housing Census, General Authority for Statistics; **C** Background: Sentinel 2 — US Geologic Survey (Earth Explorer (USGS)) website
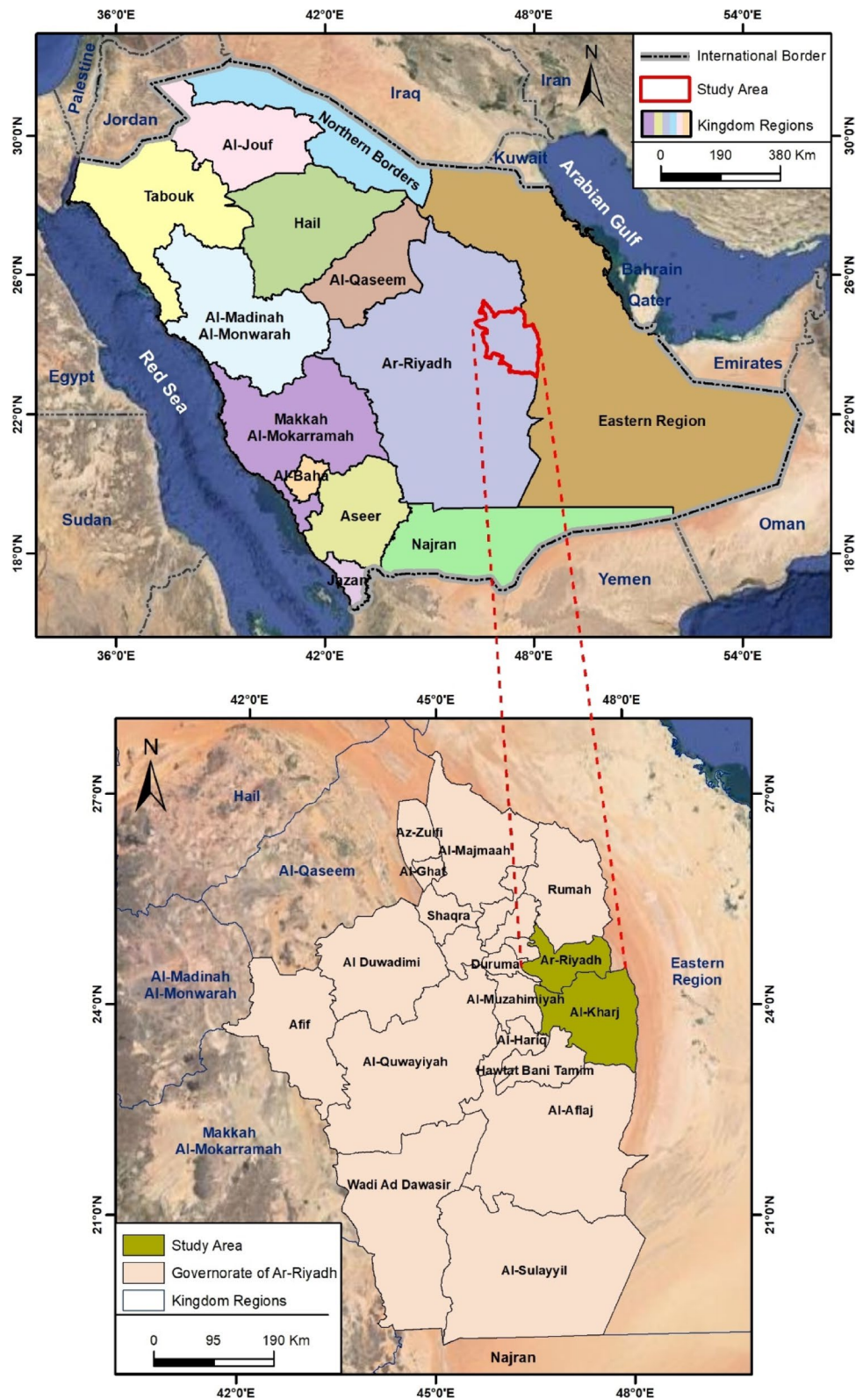
spectral. The appropriate ranges have been selected in the fields of red–green–blue. When modifying spectral ranges, they appear in different colors. For example,

in the American satellite Land sat 4–5-7, when selecting the fifth, fourth, and second ranges in the fields of Layer 1-Layer 2-Layer 3, features appear in their natural

Fig. 2 Geographical distribution of the urban communities in the rural–urban continuum axis between Ar-Riyadh and Al-Kharj Source: Sentinel 2 — with a resolution of 10-m — US Geologic Survey (Earth Explorer (USGS)) website
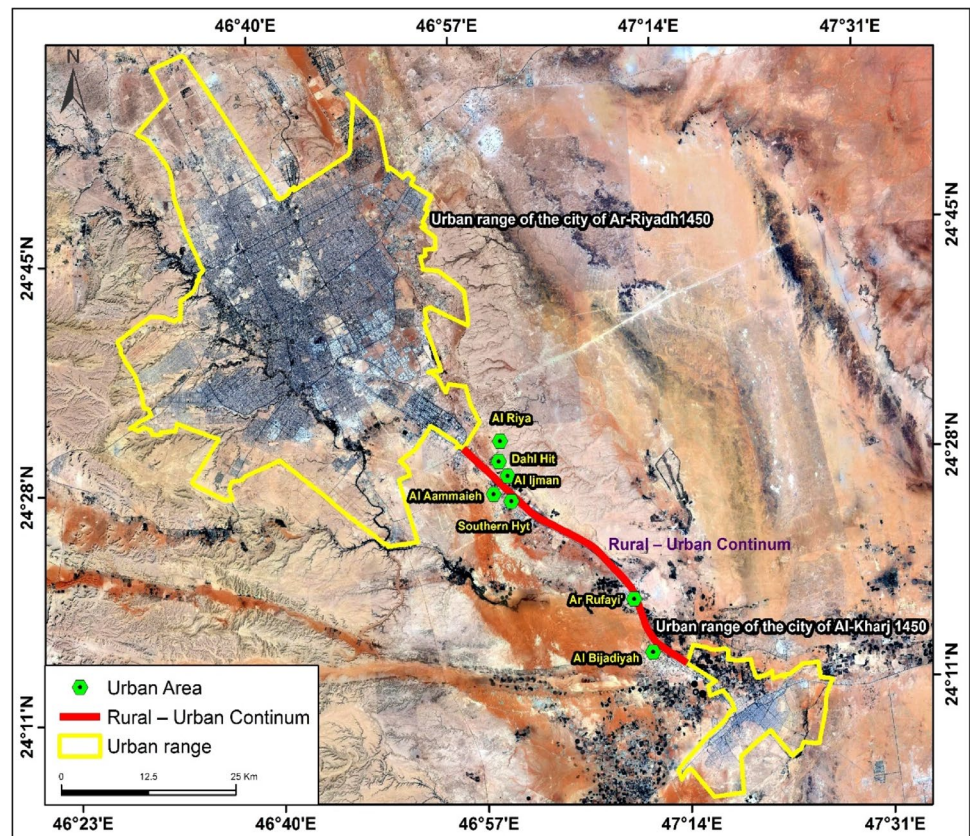
colors. However, in the American satellite Landsat 8, the sixth, fifth, and third ranges are selected in the fields of Layer 1-Layer 2-Layer 3.

The third stage: spectral enhancement

Due to some spectral interference in Landsat images, spectral enhancement of an image is performed to increase its spectral accuracy and ease of processing, as there may be problems or interference in spectral signatures. Spectral enhancement of an image is performed to increase its spectral accuracy and reduce spectral interference through principal component.

The fourth stage: spectral sections

The spectral sections of the different feature were extracted from the satellite image of the rural–urban continuum. The aim was to know the path of the spectral signatures of each feature in the different ranges of the satellite image, to know the extent of homogeneity or incongruity, and to identify the extent of conformity with reality. That was done through Spectral Profile.

The fifth stage: spectral signature

The stage of spectral signature is one of the most important stages that help to classify satellite images accurately. Several distributed samples of the spectral signatures of different feature are taken, and then similar spectral signatures are determined. This is done through

Signature Editor, which is used to take spectral signatures. Then, the spectral signature window appears.

Therefore, the spectral signature of each feature is taken through the drawing tools in the Drawing menu, and a number of spectral signatures of each feature are drawn and merged together into one spectral signature indicating the average spectral signatures taken.

The sixth stage: supervised classification

The process of supervised classification helps to standardize, identify, and separate the feature from the satellite image. After determining the spectral signatures of different feature, the image has been classified into color categories illustrating the different uses of land, which makes it easy to measure and calculate the areas of each classification. Supervised classification is done through maximum likelihood.

The seventh stage: accuracy assessment

Accuracy assessment of rural–urban continuum axis between Ar-Riyadh and Al-Kharj images was done to know the levels of trust in classifications during different years, and this was done through the following steps:

The classification and the satellite image for each year were added together in two Viewer display spaces. The classification accuracy was performed through Accuracy Assessment, the classification path which was required

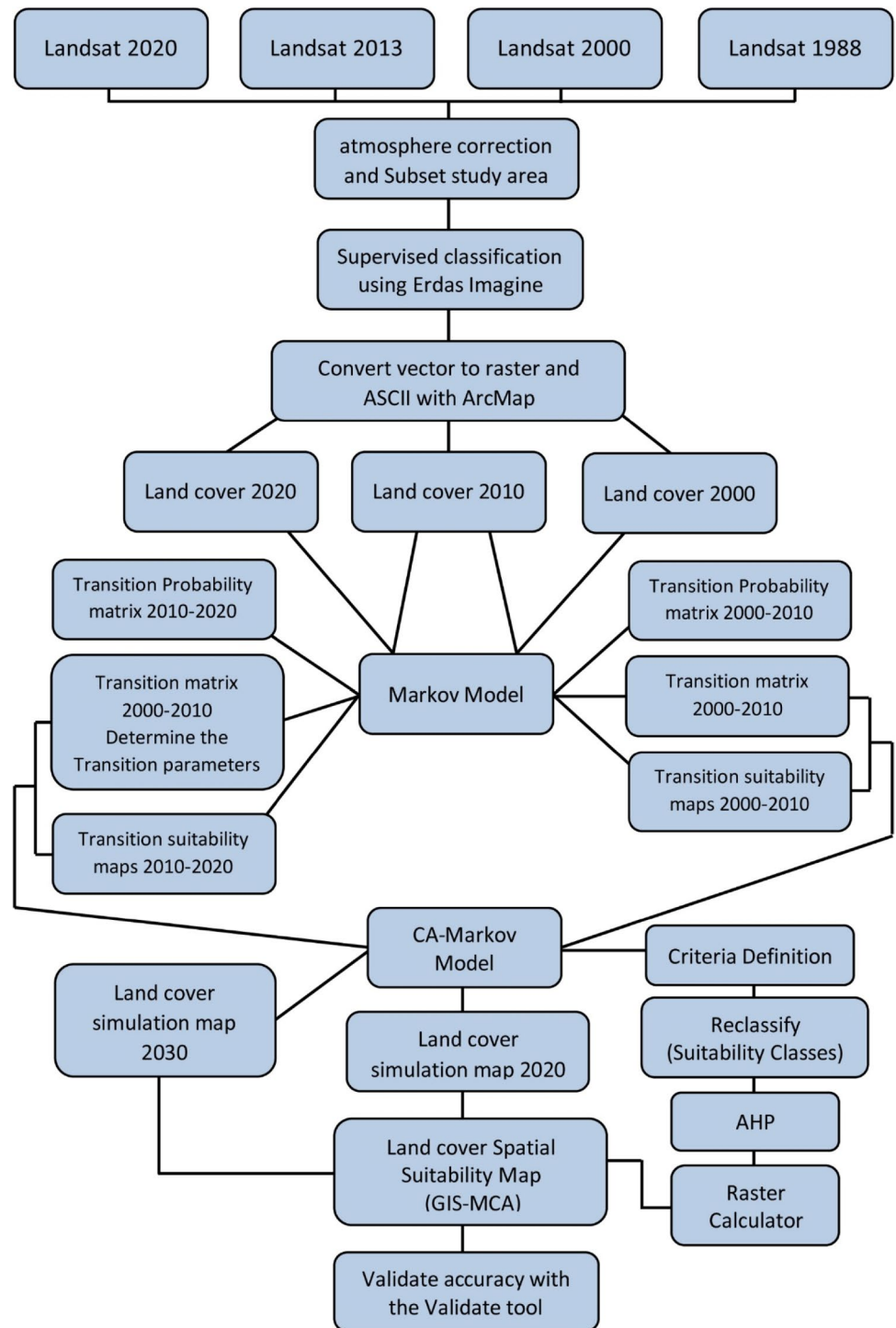**Fig. 3** Study procedures and data processing

Table 1 Characteristics of the satellite images used in monitoring the urban changes of the urban rural continuum axis from 1988 to 2020

Satellite	Sensor	Spatial resolution	Spectral bands	Path	Row	Acquiring date
Landsat 4–5	TM	30 m	8	165	43	1988
Landsat 4–5	TM		8			2000
Landsat 8	OLI		11			2013
Landsat 8	OLI		11			2020

Fig. 4 Landsat satellite images: **A** 1988, **B** 2000, **C** 2013, **D** 2020
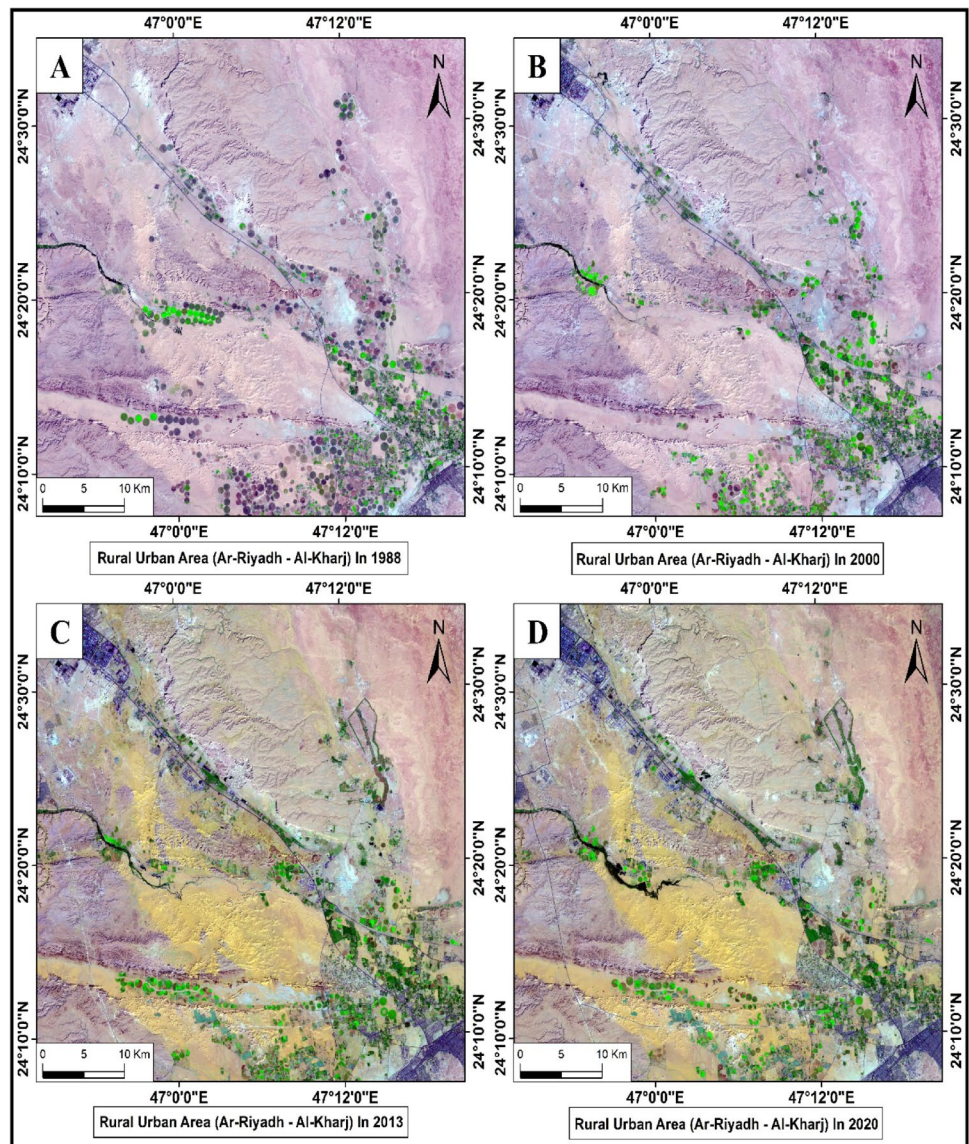
to be tested for accuracy was determined, Random Points which were used in the classification accuracy-test were added (the number of Random Points = 100 points), and then the Random Points bearing the value (zero) that reflected the unclassified areas were deleted. All unclassified samples were removed, and each point of the satellite image was tested, and the rank of the feature in which it was located was written according to the ranks upon which the classification was established.

Field samples were collected to increase the accuracy of validation of classified maps by comparing samples from the classified image with the field samples collected. Field samples were collected by GPS. The total number of field samples that were collected was 84 samples out of a total of 100 randomly distributed samples in the program (after deleting 16 samples in the unclassified areas). The field samples were distributed over the land uses in the area as

follows: agriculture (22), urban (16), desert (39), water (4), roads (3). The validation process with field samples went through several stages. In the first stage, the land use of each of the samples was collected in the field by means of the global positioning systems (GPS) through the coordinates of each sample, and in the second stage, the field samples were compared with the same samples on the original satellite image. In the third stage, field samples were compared with same samples on the classified map by the Accuracy Assessment window within the ERDAS aerial imagery and satellite image processing program. This method of accuracy validation increased confidence in the final results of the classified maps and their matching with the satellite images and reality.

The final report appears with all its details, in which the total accuracy of the classification and the classification

accuracy of each feature appear; overall accuracy (Eq. 1) and the Kappa coefficient were calculated as shown in Table 2.

$$\text{Overall accuracy} = \frac{\sum_{i=l}^{K} xil}{N} \qquad (1)$$

Where:

N = total number of samples.

$\sum_{i=l}^{K} xil$ = sum of integer samples for all classified land cover.

The satellite image classification in 1988 for the rural–urban continuum (Ar-Riyadh-Al-Kharj) reached about 99% of the total samples used in the test, which were 100 samples. That is, only one sample from the total number of samples differed in classification by 1% when assessing the accuracy, and the accuracy in 2000 AD reached about 98% of the total samples used in the test, which were 100 samples. That is, only two samples from the total number of samples differed in classification by 2% when assessing accuracy. Moreover, the accuracy in 2013 was about 97% of the total number of samples used in the test, which were 100 samples. That is, only three samples of the total number differed in classification by 3% when assessing accuracy, and the accuracy in 2020 AD reached about 99% of the total samples used in the test, and the number was 100 samples, meaning that only one sample from the total number differed in classification by 1% when assessing accuracy.

Multi-criteria analysis based on geographic information systems and determination of weights using analytic hierarchy process

Criteria definition

The first stage of multi-criteria decision analysis (MCDA) is concerned with combining information and data from several criteria for decision-making purposes (Abudeif et al. 2015). The suitable areas for future land cover using the GIS-MCA were determined using twelve criteria, namely, light slopes (S) and distance from Wadis (V), proximity to urban agglomerations (U), proximity to road network (R),

proximity to railways (RW), distance from agricultural land (A), soil type (SO), geology (G), dimension from faults (C), distance from wells (W), distance from environmental areas (E), distance from power lines (P). The main purpose of using MCA is to improve the ability of the CA-Markov cellular model to predict the future of land cover in 2030 using twelve criteria. Figures 5, 6, and 7 illustrate the criteria affecting land cover within the CA–Markov model.

Determine the input data, spatial accuracy, and sources used in the study

To conduct GIS-MCA analysis in the rural–urban continuum between Ar-Riyadh and Al-Kharj cities, the necessary data was obtained from several different sources with standardization of measurements and projections for it so that data integrates within the geographic information systems; data from different sources were collected to cover all the information about the twelve criteria; five topographic maps with scale 1:50,000 and the geologic map number (GM-121 C) of Ar-Riyadh sheet with scale 1:250,000 were obtained from the General Authority for Geologic Survey, and digital elevation model (DEM) data with resolution of 12 m was obtained from the (Vertex) website of NASA. Landsat-OLI 8 satellite image for 2020 was obtained from the US Geologic Survey (USGS) website for monitoring and delineating the agriculture areas, urban areas, and other features that might be of interest to the study; the Atlas maps of the regional planning of Ar-Riyadh were also implemented in the study and were obtained from the "Royal commission for Ar-Riyadh city), and the maps of the regional planning of Al-Kharj were obtained from the Ministry of Municipal and Rural Affairs of KSA. Table 3 shows the data input, types, spatial accuracy, and sources.

Determine the preferences values and the relative weights of the criteria

The research applied the analytic hierarchy process (AHP), which is one of the techniques used in multi-criteria decision analysis (MCDA), where the analytic hierarchy

Table 2 Accuracy assessment of satellite images from 1988 to 2020

Land cover	1988		2000		2013		2020	
	Producer	User	Producer	User	Producer	User	Producer	User
Agricultural lands	100	100	100	100	90	100	100	100
Urban areas	87.5	100	100	100	100	100	100	100
Desert lands	100	95.3	98.9	95	98	95	100	100
Water	100	100	100	100	100	100	100	100
Roads	100	100	100	100	100	100	100	100
Total accuracy	99		98		98.8		100	
Kappa coefficient	0.94		0.94		0.93		1	

Fig. 5 Unifying standards values (roads-railway-urban-slopes) using fuzzy logic on a scale ranging from (1 to 10) within CA-Markov software
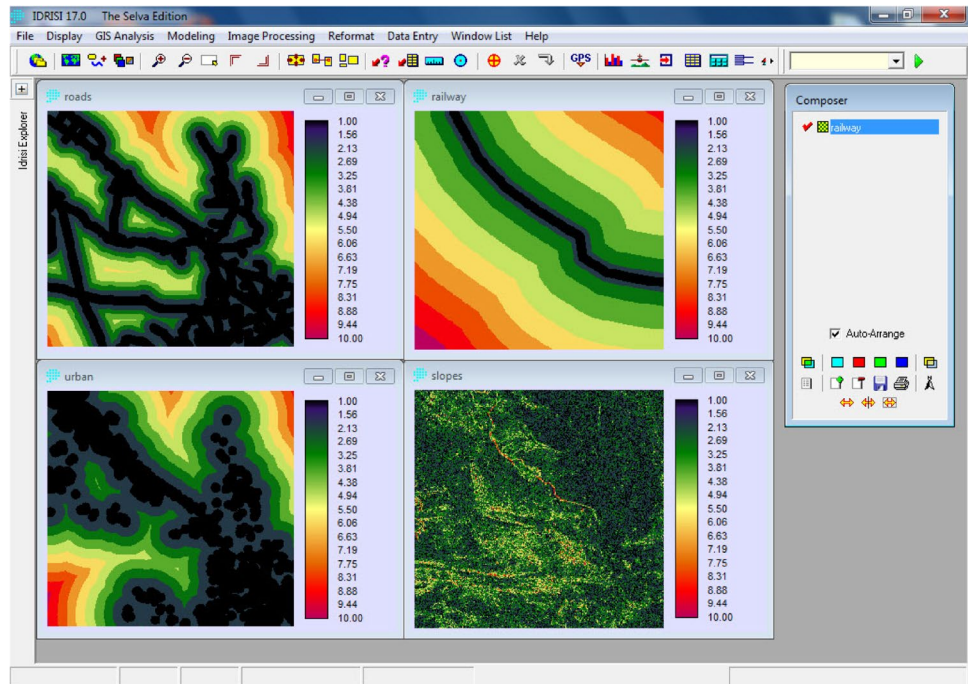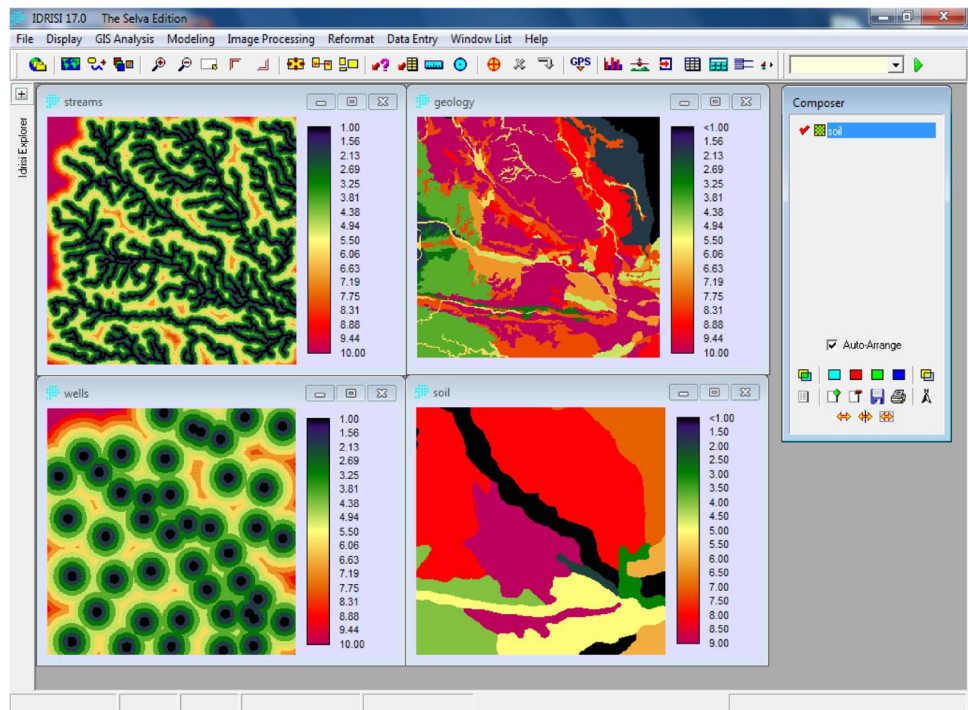
Fig. 6 Unifying standards values (streams-geology-wells-soil) using fuzzy logic on a scale ranging from (1 to 10) within CA-Markov software

process starts placing the elements of the problem at hand hierarchically, makes a pairwise comparison between them based on the selection criteria, and then weighs them in relation to the goal. Preference is based on the comparison scale suggested by Saaty (Saaty 1980). Through bilateral comparisons, we get the weight of the criteria used in prioritization. Then, there is the consistency verification,

which guarantees there are no contradictory views, and it should not exceed 10%. Tables 4, 5, and 6 show the determination of the criteria weights using AHP method.

To determine the preference values of the criteria using the hierarchical analysis method (AHP), Eqs. (2–4) were used next:

Fig. 7 Unifying standards values (agriculture-power line-crevasses-environment are) using fuzzy logic on a scale ranging from (1 to 10) within CA-Markov software
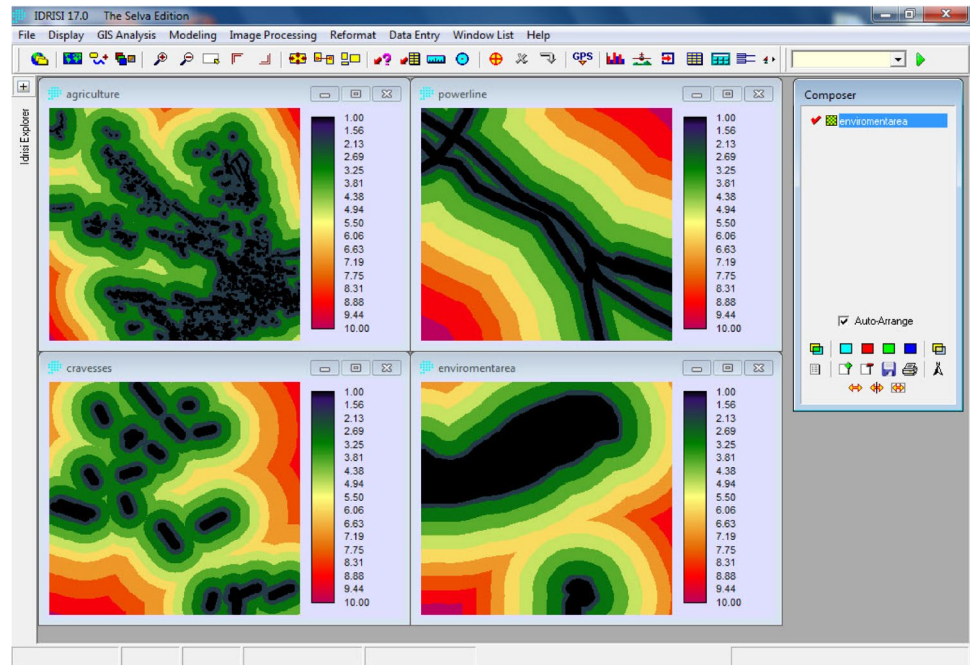

Table 3 The input data, spatial accuracy, and sources used in the study

M	Input data	Scale and spatial accuracy	Source
1	Geologic formation	Scale 1:250,000	General Authority for Geologic Survey
2	Soil	Scale 1:250,000	Ministry of Environment Water and Agriculture
3	Streams/valleys	DEM 12 m	(Vertex) Website of NASA
4	Slopes	DEM 12 m	(Vertex) Website of NASA
5	Agriculture areas	Satellite image Landsat 8/OLI	US Geologic Survey (USGS) website
6	Urban areas	Satellite image Landsat 8/OLI	US Geologic Survey (USGS) website
7	Road networks	Satellite image Landsat 8/OLI	US Geologic Survey (USGS) website
8	Railways	Regional Plan atlas for Ar-Riyadh region	Royal commission for Ar-Riyadh city—2019
9	Wells	topographic maps scale 1:50,000—Regional Plan atlas for Ar-Riyadh region	General Authority for Geologic Survey—Royal commission for Ar-Riyadh city—2019
10	Power lines	Topographic maps scale 1:50,000	General Authority for Geologic Survey
11	Crevasses/faults	Topographic maps scale 1:50,000	General Authority for Geologic Survey
12	Environmental areas	Topographic maps scale 1:50,000	General Authority for Geologic Survey

$$[a_{ij}], \text{ where } i, j = 1, 2, \ldots ..n \tag{2}$$

$$a_{ij} = 1 \text{ f or } i = j \tag{3}$$

$$a_{ij} = \frac{1}{a_{ji}} \text{f or } i \neq j \tag{4}$$

The percentage of preference values between two parameters, one in a column and the other in a row, can be determined using the formula:

$$\bar{a}_{jk} = \frac{a_{jk}}{\sum_{1=I}^{m} a_{Ik}} \tag{5}$$

Where:

$\bar{a}_{jk}$: the percentage of preference between two parameters in column and row.

a_{jk}: the values of preference between two parameters in column and row.

$\sum_{1=I}^{m} a_{Ik}$: the total sum of the column parameter.

Table 4 The preferences values of the criteria using the AHP method

Service	S	V	U	R	RW	A	SO	G	C	W	E	P
S	1	1	2	3	4	5	6	6	7	8	9	9
V	1	1	2	3	4	5	6	6	7	8	9	9
U	0.5	0.5	1	2	3	4	5	5	6	7	8	8
R	0.33	0.33	0.5	1	2	3	4	4	5	6	7	8
RW	0.25	0.25	0.33	0.5	1	2	3	3	4	5	6	7
A	0.2	0.2	0.25	0.33	0.5	1	2	2	3	4	5	6
SO	0.17	0.17	0.2	0.25	0.33	0.5	1	1	2	3	4	5
G	0.17	0.17	0.2	0.25	0.33	0.5	1	1	2	3	4	5
C	0.14	0.14	0.17	0.2	0.25	0.33	0.5	0.5	1	2	3	4
W	0.13	0.13	0.14	0.17	0.2	0.25	0.33	0.33	0.5	1	2	3
E	0.11	0.11	0.13	0.14	0.17	0.2	0.25	0.25	0.33	0.5	1	2
P	0.11	0.11	0.13	0.13	0.14	0.17	0.2	0.2	0.25	0.33	0.5	1
Sum	4.11	4.11	7.05	10.97	15.92	21.95	29.28	29.28	38.08	47.83	58.5	67

Table 5 The percentages of the preferences values using the AHP method

Service	S	V	U	R	RW	A	SO	G	C	W	E	P
S	0.243	0.243	0.284	0.273	0.251	0.228	0.205	0.205	0.184	0.167	0.154	0.134
V	0.243	0.243	0.284	0.273	0.251	0.228	0.205	0.205	0.184	0.167	0.154	0.134
U	0.122	0.122	0.142	0.182	0.188	0.182	0.171	0.171	0.158	0.146	0.137	0.119
R	0.080	0.080	0.071	0.091	0.126	0.137	0.137	0.137	0.131	0.125	0.120	0.119
RW	0.061	0.061	0.047	0.046	0.063	0.091	0.102	0.102	0.105	0.105	0.103	0.104
A	0.049	0.049	0.035	0.030	0.031	0.046	0.068	0.068	0.079	0.084	0.085	0.090
SO	0.041	0.041	0.028	0.023	0.021	0.023	0.034	0.034	0.053	0.063	0.068	0.075
G	0.041	0.041	0.028	0.023	0.021	0.023	0.034	0.034	0.053	0.063	0.068	0.075
C	0.034	0.034	0.024	0.018	0.016	0.015	0.017	0.017	0.026	0.042	0.051	0.060
W	0.032	0.032	0.020	0.015	0.013	0.011	0.011	0.011	0.013	0.021	0.034	0.045
E	0.027	0.027	0.018	0.013	0.011	0.009	0.009	0.009	0.009	0.010	0.017	0.030
P	0.027	0.027	0.018	0.012	0.009	0.008	0.007	0.007	0.007	0.007	0.009	0.015
Sum	1	1	1	1	1	1	1	1	1	1	1	1

Table 6 The relative weights of criteria for determining future land cover for the rural–urban continuum axis between Ar-Riyadh and Al-Kharj

Service	Sum of the row	The relative weight
S	2.572	0.214
V	2.572	0.214
U	1.840	0.153
R	1.354	0.113
RW	0.990	0.082
A	0.714	0.059
SO	0.504	0.042
G	0.504	0.042
C	0.354	0.030
W	0.258	0.022
E	0.188	0.016
P	0.151	0.013
Sum	12	1

The relative weight values are determined using the formula:

$$w_j = \frac{\sum_{1=I}^{m} a_{jl}}{m} \tag{6}$$

Where:

w_j: the value of the relative weight for the row parameter.

$\sum_{1=I}^{m} a_{jl}$: sum of the percentages of the preference values for a row parameter.

m: the final value of the sum $\sum_{1=I}^{m} ajl$ for all rows.

Table 7 shows the final weights.

The consistency is computed using the formula:

$$CI = \frac{\lambda Max - n}{n - 1} \tag{7}$$

Where

$ʎMax$: the square root of the pairwise comparison matrix mean.

Table 7 Random stability index

N	1	2	3	4	5	6	7	8	9	10
R	0	0	0.52	0.89	1.11	1.25	1.3	1.4	1.45	1.49

n: the number of parameters or criteria

$$CI = \frac{8.7 - 8}{8 - 1} = 0.1 \qquad (8)$$

The closer the result to zero, the more confident the consistency index and vice versa.

Secondly, calculating the consistency index percent from the formula:

$$Stability\ ratio = \frac{CI}{R} \qquad (9)$$

where R is the random consistency index based on the number of criteria taken from Table 6.

The value of the random consistency index based on the previous table is equal to 1.49; that is because the used criteria are more than 10. The percent of the consistency index is $0.07/1.49 = 5\% = 0.05$. The consistency values must be in consistent range not exceeding 0.1 (i.e., 10%), as the higher the value than 0.1, the more conflict in consistency.

Using the Cellular Automata Markov model to predict land cover in 2030

The prediction of future land cover was performed with IDRISI Selva software version 17.0 using the CA-Markov prediction model; IDRISI software also enables the implementation of CA–Markov model, which combines local cellular behavior and Markov chain analysis; multi-criteria evolution (MCE) analysis; multi-objective land allocation (MOLA); the procedures of land-cover prediction, which add an element of the spatial continuum; and the potential spatial distribution of transitions to Markov chain analysis.

The supervised images were exported to IDRISI Selva software to apply the CA-Markov prediction model to model and simulate the land cover in the study area in 2030 as follows:

1. The Markov model was used to get the transition probability matrix and transition area matrix for the time period 2000–2010.Predicting the land cover in 2020 was obtained using the CA–Markov model which required:

   The 2010 land cover images
   The transition area matrix (obtained in the previous step)
   The number of iterations was determined to 10 iterations (according to the number of years desired)

   The default 5 × 5 filter
   A default error rate of zero

2. A comparison of the actual supervised image in 2020 and the predicted image obtained from the CA-Markov using the "validate simulation determination tool" in IDRISI Selva. The validation step was required to be assured of the results that will be obtained for the simulation of 2030.

3. Prediction of land cover in 2030 using the CA-Markov based on the spatial suitability map using GIS-MCA and AHP (Figs. 8 and 9); the number of iterations was determined to 10 (years from, 2020 to 2030), filter of 5 × 5, and a zero error rate.

Results and discussion

Monitoring of the land cover changes of the rural – urban continuum axis between Ar-Riyadh and Al-Kharj during the period 1988–2020

Monitoring of the changes in the area of agricultural lands during the period 1988–2020

The analysis of Table 8 revealed that, the area of agricultural lands in 1988 amounted to about 224.02 km², representing about 8.2% of the total area of the study area. In the year of 2000, the agricultural lands decreased to 126.98 km², which constitutes about 4.7% of the total area of the study area, while it increased in the year of 2013 to 166.18 km², representing about 6.1%. Then, it decreased again in the year of 2020 to reach 162.9 km², representing about 6% of the total area. From the analysis of the agricultural lands from 1988 to 2020, it is clear that the annual growth rate was about -0.99% and the average annual decline was -1.9 km², which means that the rural–urban continuum (Ar-Riyadh-Al-Kharj) lost about 61 km² of its agricultural lands. Figure 10 shows the change in the agricultural areas of the rural–urban continuum during the period 1988–2020.

The bulldozing of agricultural lands to establish industrial zones helped to lose a lot of agricultural land. In addition, the great housing crisis in the city of Ar-Riyadh led to search for areas that are less expensive and close to the city, and many agricultural lands have been transformed into urban areas to meet the needs of housing demand. The ease of

Fig. 8 Spatial suitability of the criteria affecting the rural–urban continuum axis between Ar-Riyadh and Al-Kharj: **A** valleys, **B** land surface inclinations, **C** road networks, **D** urban communities, **E** agricultural lands, **F** railways
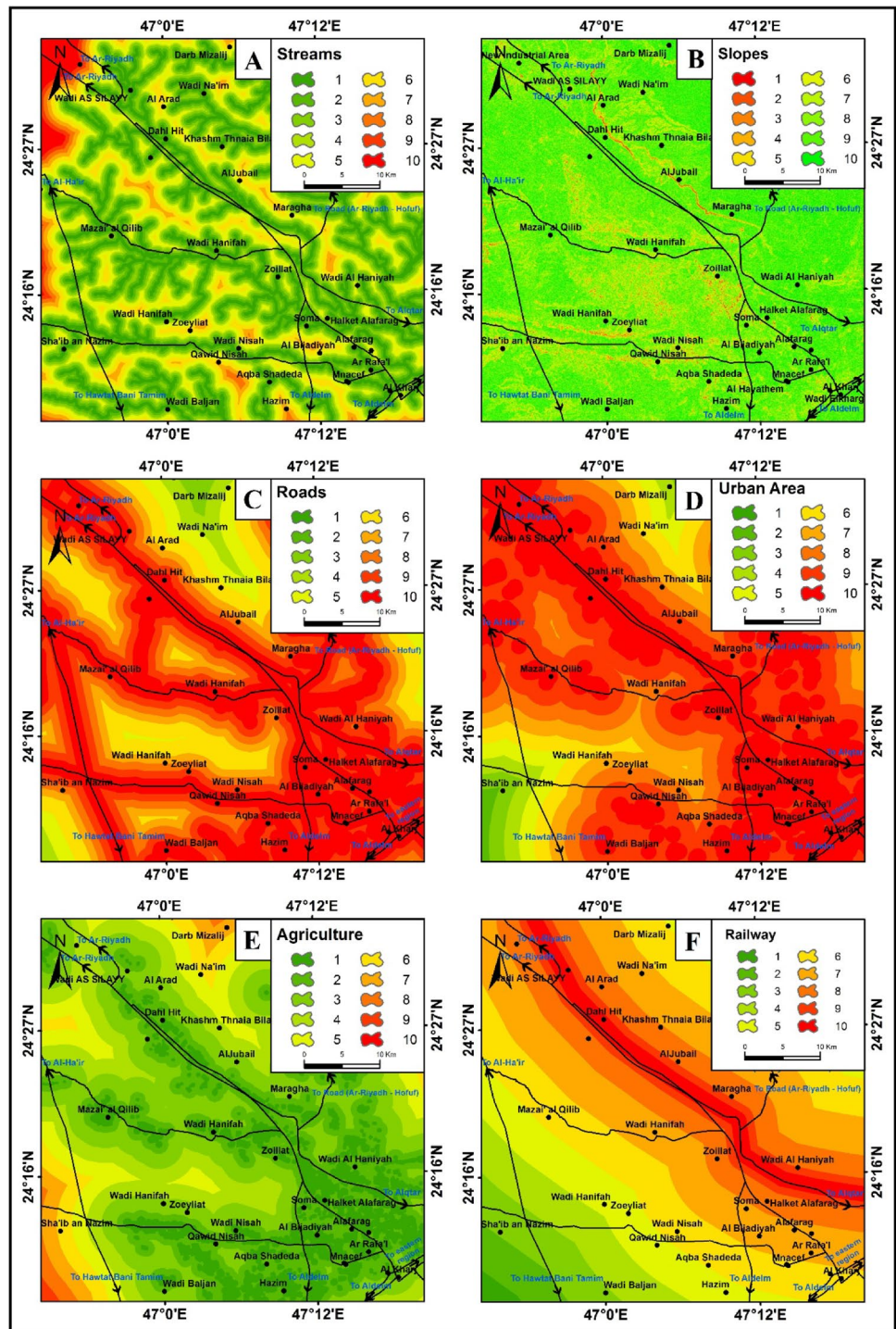

spreading agricultural rest houses along the Ar-Riyadh-Al-Kharj corridor helped in converting these rest houses into accommodation for those looking away from the city noise and crowding, and the establishment of the industrial zone south of Ar-Riyadh helped to attract investors to establish other industries near these areas, and then much of the agricultural land was lost.

Monitoring of the urban areas changes from 1988 to 2020

From Table 9, it is clear that the urban areas in the year of 1988 were about 36.25 km^2, which represents 1.3% of the total area. It increased to 49.92 km^2 in the year 2000, which constitutes about 1.8% of the total area. It increased to 90.92 km^2 in 2013, which is equivalent to 3.3% of the

Fig. 9 Spatial suitability of the criteria affecting the rural–urban continuum axis between Ar-Riyadh and Al-Kharj: **A** geology, **B** soil, **C** faults, **D** water sources, **E** power lines, **F** environmental areas
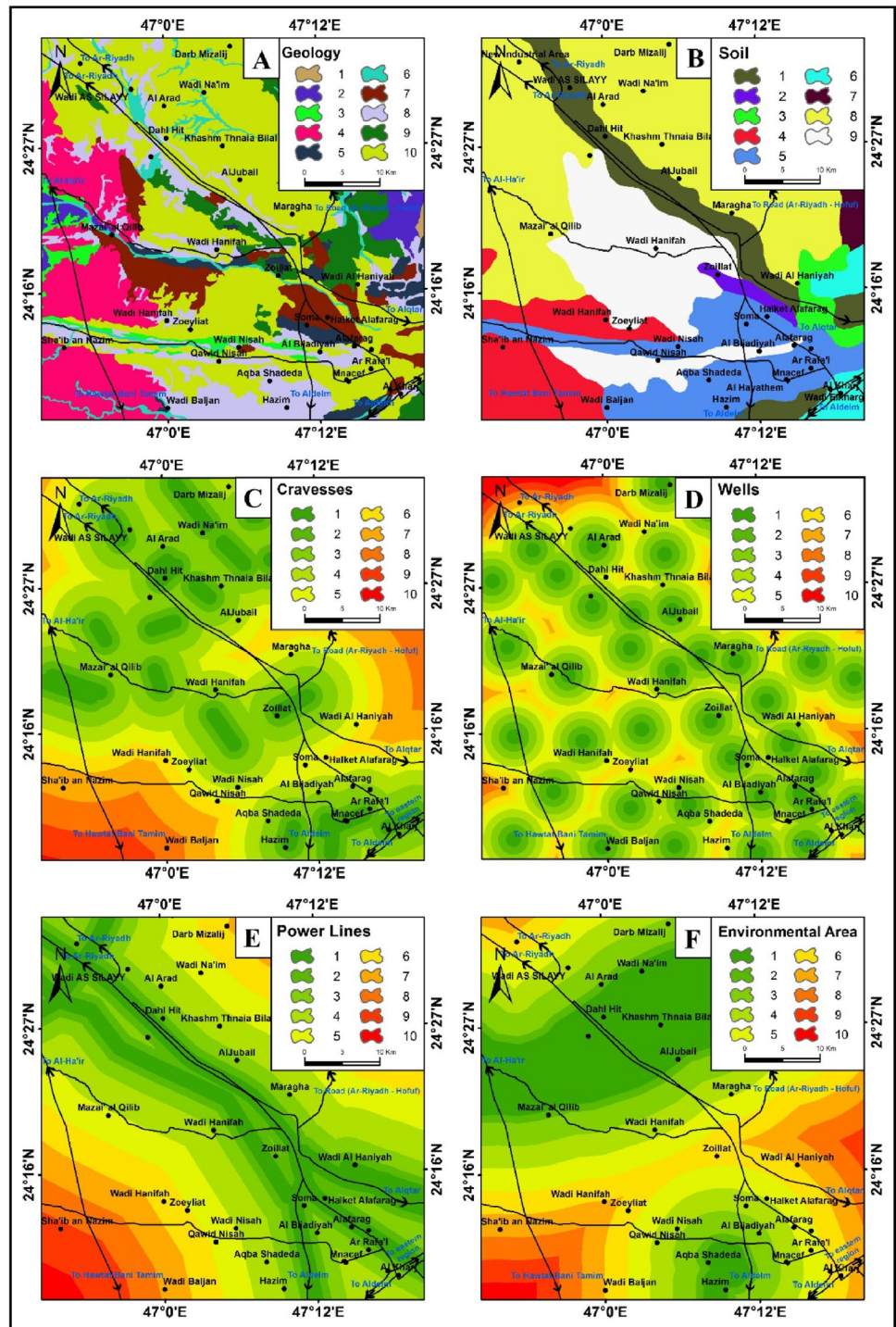
total area, and it continued to rise in the year of 2020 and amounted to 114.09 km², with nearly 4.2% of the total area.

The analysis of Table 8 revealed that the annual growth rate during the period from 1988 to 2020 reached 3.65%, and the average annual increased to 2.4 km². That is, the urban–rural continuum axis between Ar-Riyadh and Al-Kharj has achieved an increase 78 km² in the urban areas.

Monitoring of the desert land changes during the period 1988–2020

Table 10 shows the changes in desert lands from 1988 to 2020. The desert areas in 1988 represented about 2444.51 km², and it increased to reach 2527.84 km² in 2000 with an

Table 8 Changes in the agricultural lands of the rural–urban continuum axis during the period 1988–2020

Year	Area (km²)	Area (km²)		1988	Increase of annual average	Rate of average increase	Rate of change
		km²	%				
1988	224.02						
2000	126.98	− 97.0	− 59.57%	− 43.32%	− 8.1	− 4.62%	− 43.32%
2013	166.18	39.2	24.06%	17.50%	3.0	2.09%	30.87%
2020	162.9	− 3.3	− 2.01%	− 1.46%	− 0.5	− 0.28%	− 1.97%
2020–1988		− 61.1	− 37.52%	− 27.28%	− 1.9	− 0.99%	− 37.52%

Fig. 10 Land cover for the rural–urban continuum axis: **A** in 1988, **B** in 2000, **C** in 2013, **D** in 2020
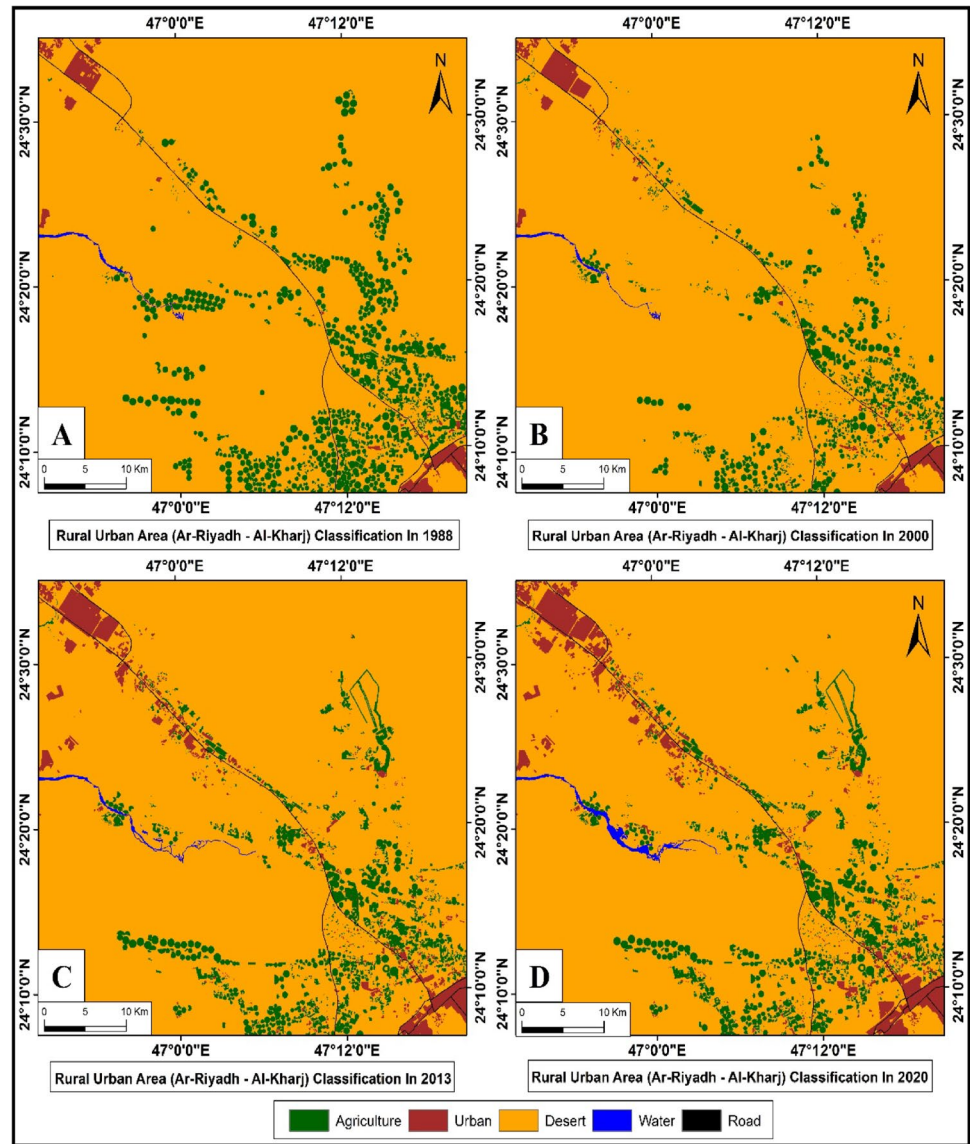
increase of 103.41%. During the period from 2000 to 2013, it reached about 2445.27 km² in 2013 with a decrease of 96.73%. Then, the desert lands decreased about 2420.43 km² in 2020 with 98.98% than it was in 2013.

Monitoring of the changes in water during the period 1988–2020

Table 11 presents the changes in water; their areas in 1988 were about 4.77 km², the area reached 4.8 km² in 2000, and it increased to 7.18 km² in 2013 with an increase

Table 9 Changes in the urban areas of the rural–urban continuum axis during the period 1988–2020

Year	Area (km²)	Area (km²)		1988	Increase of annual average	Rate of average increase	Rate of change
		km²	%				
1988	36.25						
2000	49.92	13.7	11.98%	6.10%	1.1	2.70%	37.71%
2013	90.92	41.0	35.94%	18.30%	3.2	4.72%	82.13%
2020	114.09	23.2	20.31%	10.34%	3.3	3.30%	25.48%
2020–1988		77.8	68.23%	34.75%	2.4	3.65%	68.23%

Table 10 Changes in the desert lands of the rural–urban continuum during the period 1988–2020

Year	1988	2000	2013	2020
Desert areas (km²)	2444.51	2527.84	2445.27	2420.43

Table 11 Changes in the water areas of the rural–urban continuum during the period 1988–2020

Year	1988	2000	2013	2020
Water (km²)	4.77	4.8	7.18	12.13

Predicting the future of land cover for the urban rural continuum axis (Ar-Riyadh–Al-Kharj) until 2030

The actual and predicted land cover in 2020

CA–Markov model was applied on the land cover maps obtained previously from the supervised classification of the satellite images for the years 2000 and 2010. The land cover types existed in 2000 and 2010 were agricultural lands, urban areas, desert lands, water, and roads. The two land cover layers were entered to the model, and the time interval between the two images was set to 10 indicating

Table 12 Transition probability matrix of land cover during the period 2000–2010

Year	2010				
	Land cover	Agricultural lands	Urban areas	Desert areas	Water	Roads
2000	Agricultural lands	0.7844	0.0131	0.2024	0.0000	0.0001
	Urban areas	0.0023	0.9939	0.0017	0.0000	0.0021
	Desert areas	0.0250	0.0141	0.9600	0.0009	0.0000
	Water	0.0000	0.0001	0.0266	0.9733	0.0000
	Roads	0.0000	0.0000	0.0000	0.0000	1.0000

Table 13 Transition matrix (in pixels) for different land cover from 2000 to 2010

Year	2010				
	Land cover	Agricultural lands	Urban areas	Desert areas	Water	Roads
2000	Agricultural lands	144,840	2415	37,376	0	12
	Urban areas	233	100,408	169	0	211
	Desert areas	67,937	38,237	2,608,291	2507	0
	Water	0	1	212	7766	0
	Roads	0	0	0	0	12,210

of 149.58% from what it was in 2000. In 2020, the area reached 12.13 km² with an increase of 168.94% over what it was in 2013.

the difference in years from 2000 to 2010. The number of years to be signed after the second image has been set to 10, indicating the difference in years between 2010 and 2020. So that, the model will generate a future land cover map for the year of 2020. The transition probability matrix, the transition areas matrix, and the transition suitability maps are obtained in Tables 12 and 13. The subsequent step was comparing the predicted map with the actual land cover in

2020, which obtained supervised classification of the satellite images for the years 2020. The aim of the comparison between the actual and predicted land cover map in 2020 was to verify the accuracy of the model to be assured of the results of the forecast in 2030.

The CA–Markov model was run for the second time using the classified images in 2010 and 2020, the number of iterations was set to 10 (number of years between 2010 and 2020) to get the simulated land cover map for the year 2020. Figure 11 shows the actual and predicted land cover maps in year 2020. Table 14 presents the areas of

the land cover in the actual and predicted land cover maps in year 2020.

Table 14 shows the accuracy of the prediction model, which was ranged between 82.8 and 98.91%. for different land cover. The total area of agricultural lands resulting from the predicted map in 2020 was about 190.9 km^2, while the actual total area resulted from the supervised classification was 162.9 km^2, with an accuracy of 82.8%.

The urban areas were 126.6 km^2 in the predicted map in 2020, while the actual area was 114.09 km^2, with an accuracy of 89.03%. The desert lands were 2381.5 km^2 in the predicted map in 2020, while the actual area was 2420.43 km^2, with an accuracy of 98.39%. The total area of water in the predicted map was 10.4 km^2, and its actual area was 12.13 km^2 with accuracy reached 85.74%. Finally, the total area of the main roads in the prediction map was 11.1 km^2, while the actual area was 10.98 km^2 and the accuracy was 98.91%.The validate tool was used in the IDRISI program as second method to verify the accuracy of the CA-Markov prediction model. Kappa value of 0 illustrates agreement between actual and reference map (equals chance agreement), the upper and lower limit of kappa is $+1.00$ (occurs when there is total agreement) and -1.00 (represents agreement which is less than chance) (Congalton 1991). The results of the validate tool showed very high accuracy for the various Kappa coefficients as seen in Table 14. The values of the parameter K_{no}, $K_{location}$, $K_{locationStrata}$, and $K_{standard}$ were 0.9488, 0.8717, 0.8717, and 0.8091 respectively. According to Zadbagher and Becek (2018), a model is valid if the overall Kappa ($K_{standard}$) score exceeds 70% (or 0.7). The $K_{standard}$ score, close to 90%, is a very strong indicator of the overall accuracy and performance of the model, and the remaining k scores, all exceeding 85%, indicate that there are almost no or very small quantification and location errors between the predicted and the actual land cover map for 2019. Thus, the simulation has a strong ability to predict both the quantity and the locations of change (Table 15).
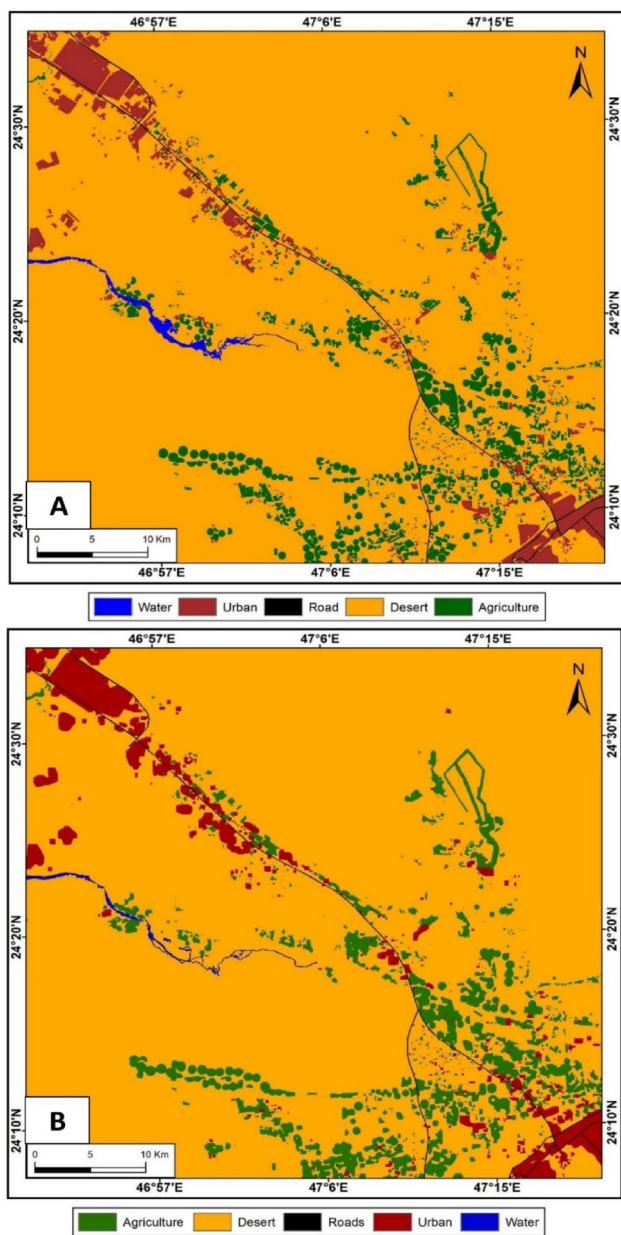

Fig. 11 A Land cover map: **A** actual in year 2020, **B** predicted land cover map in 2020

Table 14 A comparison between actual and predicted statistics in 2020 to assess the model's accuracy

Land cover	Area (km^2)		Prediction accuracy (%)
	Actual 2020	Projected 2020	
Agricultural lands	162.9	190.9	82.8%
Urban areas	144.09	126.6	89.03%
Desert lands	2420.43	2381.5	98.39%
Water	12.13	10.4	85.74%
Roads	10.98	11.1	98.91%
Total	2720.5	2720.5	100%

Table 15 Kappa coefficient to assess the accuracy of the prediction model

Kappa coefficient	Kappa coefficient value for CA-Markov
K_{no}	0.9488
$K_{location}$	0.8717
$K_{locationStrata}$	0.8717
$K_{standard}$	0.8091

Prediction of the future land cover in the year of 2030

A Markov model was run using the supervised images 2010 and 2020; the time interval between the two images was set to 10, indicating the 10-year difference between the two images. The number of years to be signed after the second image has been set to 10, indicating the 10-year difference from 2020 to 2030. The number of iterbations was set to be 10 equal to the number of years to be predicted. The transition probability matrix and the transition areas matrix are illustrated in Tables 16 and 17 respectively.

The spatial suitability map was obtained using the multi-criteria analysis (GIS-MCA) and hierarchical analysis (AHP). From Fig. 12 and Table 18, it is clear that the land cover of the rural–urban continuum axis between Ar-Riyadh and Al-Kharj in 2030 is varied in terms of the amount of change expected to occur, either by increase or decrease. The urban land cover was the most likely type in terms of increasing the area (it is expected to increase from 114.09 km^2 in 2020 to 141.19 km^2 2030). The increase in the urban areas came at the expense of the desert lands. The desert lands lost about 2396.46 km^2 from its total area

in 2030 which were 2420.43 km^2 in 2020 with a decrease equal to 23.97 km^2. The agricultural lands recorded an expected decrease in the total area equivalent to 3.65 km^2 as the total area was 162.9 km^2 and 159.25 km^2 in 2020 and 2030, respectively. The change in water was about 0.4 km^2, as it recorded an area of about 12.53 km^2 in 2030 while in 2020, it was 12.13 km^2. Finally, the area of the main roads recorded a very slight increase of 0.12 km^2, as the area 2020 was 10.98 km^2 and changed to 11.1 km^2 in 2030.

Validation of spatial suitability map

From the suitability map in Fig. 13, the total area of the urban in 2030 is expected to be 141.19 km^2. The area of the urban in the very high suitability zone is 75.12 km^2, which is 53.2% of the total area of the urban in 2030, whereas the total area of the urban located in the high suitability zone is 43.98 km^2 with about 31.15% of the total area of the urban. The total area of the urban located in the moderate suitability zone is 18.88 km^2 with a ratio of 13.37%. The total area of the urban located in the low suitability zone is 3.21 km^2 with only 2.27% the total area of the urban. Table 19 shows that no urban areas located in very low suitability zone in 2030.

The results show high compatibility between the suitability map and the projected map of year 2030 where 85% of the urban areas are located in very high and high suitability zones. This indicates an excellent compatibility between suitability map and projected maps, and this confirms the effectiveness of the techniques used to get these results.

Table 16 The probability transition matrix of land cover from 2020 to 2030

Year	2030				
	Land cover	Agricultural lands	Urban areas	Desert areas	Water	Roads
2020	Agricultural lands	0.8764	0.0034	0.1184	0.0018	0.0001
	Urban areas	0.0010	0.9951	0.0039	0.0000	0.0000
	Desert areas	0.0067	0.0115	0.9791	0.0026	0.0000
	Water	0.0000	0.0001	0.1036	0.8963	0.0000
	Roads	0.0000	0.0000	0.0000	0.0000	1.0000

Table 17 Transition matrix (in pixels) for different land cover from 2020 to 2030

Year	2030				
	Land cover	Agricultural lands	Urban areas	Desert areas	Water	Roads
2020	Agricultural lands	158,638	609	21,427	331	0
	Urban areas	125	126,139	498	0	0
	Desert areas	18,106	30,972	2,633,191	7097	0
	Water	0	1	1397	12,085	0
	Roads	0	0	0	0	12,210

Fig. 12 Land cover in the urban–rural continuum axis between Ar-Riyadh-Al-Kharj in year 2030 based on the spatial suitability map for land cover
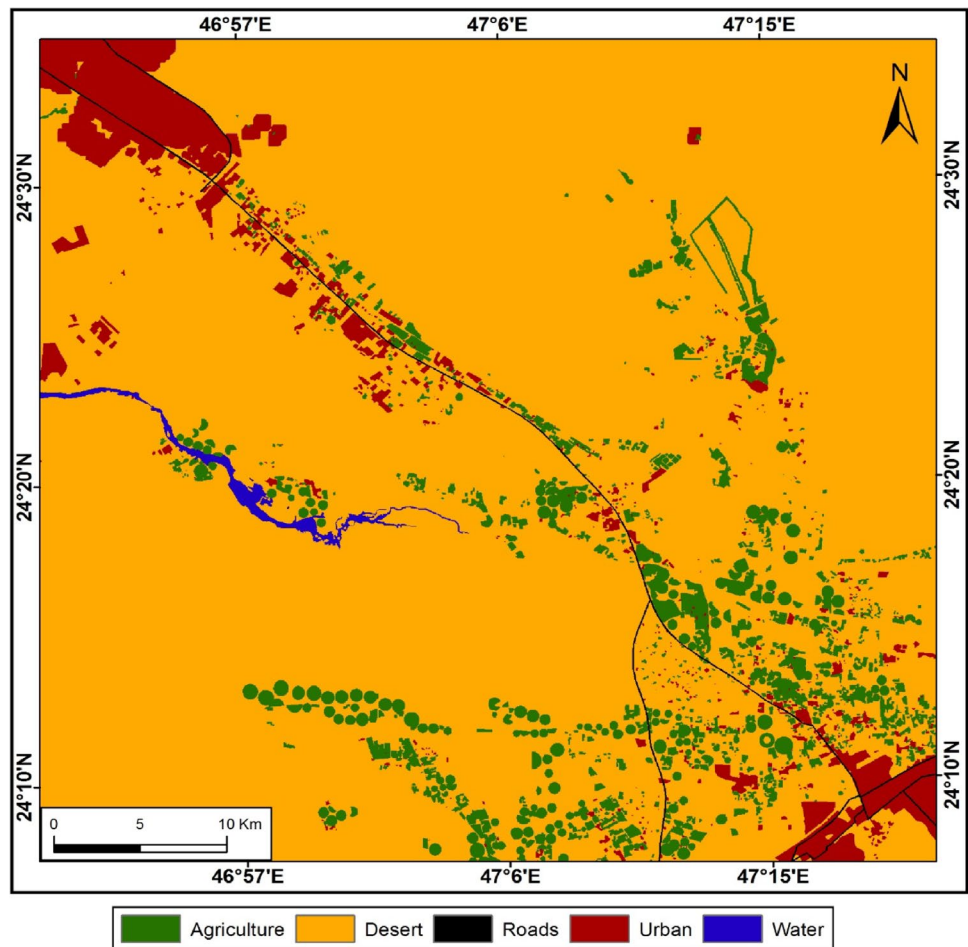

Table 18 Areas of land cover in 2020 and projected land cover in 2030

Land cover	Area (km^2)		
	2020	2030	Expected change
Agricultural lands	162.9	159.25	− 3.65
Urban areas	114.09	141.19	+ 27.1
Desert lands	2420.43	2396.46	− 23.97
Water	12.13	12.53	+ 0.4
Roads	10.98	11.1	+ 0.12
Total	2720.5	2720.5	0

Scenarios to reduce the increase of the industrial usage control in the map of using the rural–urban–continuum land in 2030

The map of using the rural–urban–continuum land for the year 2030 revealed that the industrial usage is the most likely type in terms of increasing the area and to preserve the remaining agricultural lands that have lost more than 61 km^2 during the past 30 years and which are expected to witness continued loss during the next 10 years and to reduce the increase of the industrial usage control in the map of using the rural–urban–continuum land in the year 2030; the study proposes three different scenarios so that these scenarios take into account the current conditions of land usage in the study area, especially the industrial establishments spread on the axis of the Ar-Riyadh-Al-Kharj road and its relation to the rest of usages, this as well as the link of some industries to the sites of some raw sources, as there are industries such as dates, vegetables, fruits, dairy and water that require their presence in their current locations while preserving as much as possible the agricultural lands and work to develop it and increase its productivity; the first scenario deals with moving industrial establishments towards the city of Al-Kharj in the industrial zones designated for this, and allocating the lands located on the (Ar-Riyadh-Al-Kharj) road for agricultural and recreational use and not to be extended to any other activities so that no extension occurs from the cities of Ar-Riyadh and Al-Kharj and let the Ar-Riyadh-Al-Kharj road remain a developmental separator and a barrier to urban inflation, while the second scenario concerned (keeping industrial facilities on the axis) deals with confirming the existence of industrial

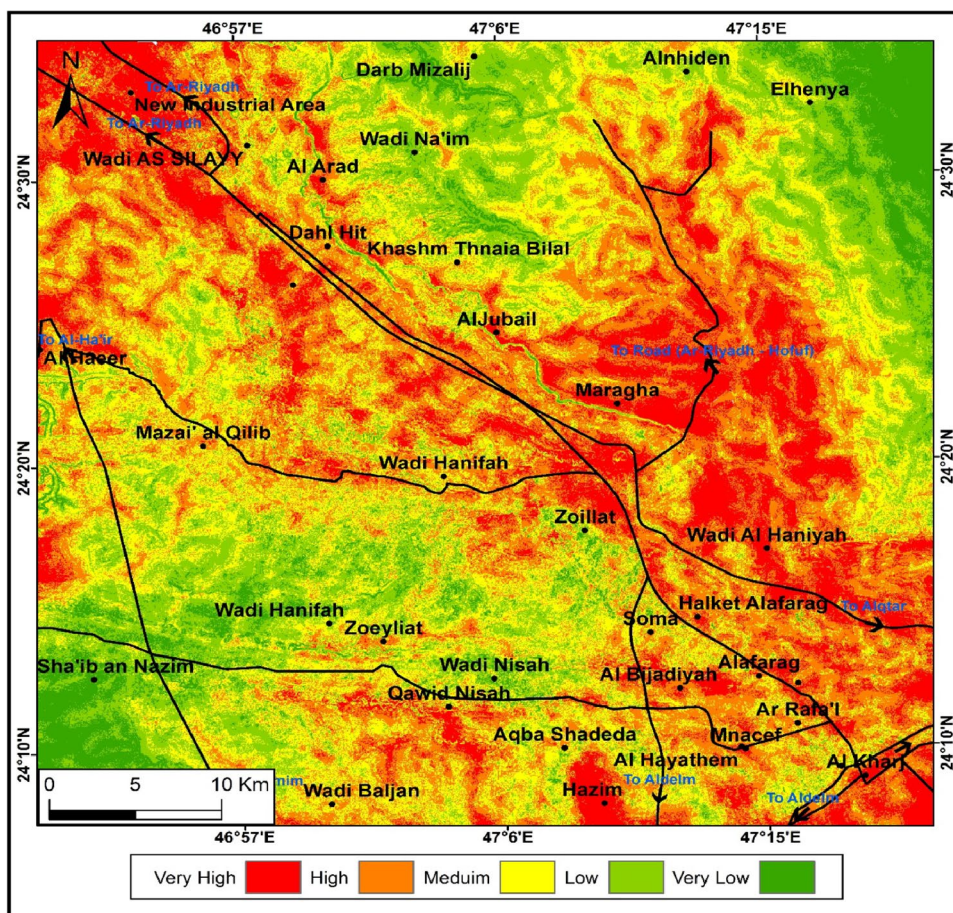**Fig. 13** Final spatial suitability map for future land cover

Table 19 Area of the spatial suitability zones for the expected urban mass in 2030

Spatial suitability zones	Area km²	Percent
Very high suitability	75.12	53.205%
high suitability	43.98	31.150%
Moderate suitability	18.88	13.372%
Low suitability	3.21	2.273%
Very low suitability	–	–
Total	141.19	100%

facilities, but with organizing them according to the foundations, standards, and planning and design controls, by choosing places linked to the Ar-Riyadh-Al-Kharj road axis, as combined industrial areas, away from the road with a suitable depth, and provided them with all necessary infrastructure, while the third scenario deals with converting sites that concentrate more than one industrial facility at the present time into an industrial cell after rehabilitating and optimization of urban spaces in it and adding other facilities, in accordance with the principles and standards followed in this regard to produce the least

losses on the material, developmental, and environmental levels (Fig. 14).

Table 20 illustrates the evaluation of scenarios to reduce the increase of industrial usage control. the scenarios to reduce the increase of the industrial usage control have been evaluated in the map of using the Rural–Urban–Continuum land in 2030, by giving points for the evaluation, which are (3,2,1,0) According to the evaluation of the scenario according to the standard, so that evaluation (0) means that the criterion is not met, and evaluation (3) means that the criterion is fully achieved.

Through the trends of each of the three expected scenarios, which represent general trends for scenarios to reduce the increase of the industrial usage control on the axis (Ar-Riyadh-Al-Kharj), it is noted that although all scenarios contribute to solving the problem, they differ in terms of economic gains. Through the evaluation of these scenarios in the previous table, the third scenario can be chosen as an optimal scenario, as it combines the advantages of the first and second scenarios, supporting the orientations of the previous plans such as the national urban strategy and the regional plan for Al-Kharj Governorate, as well as preserving as much as possible the current industrial system and reducing the resulting economic cost. For the transfer
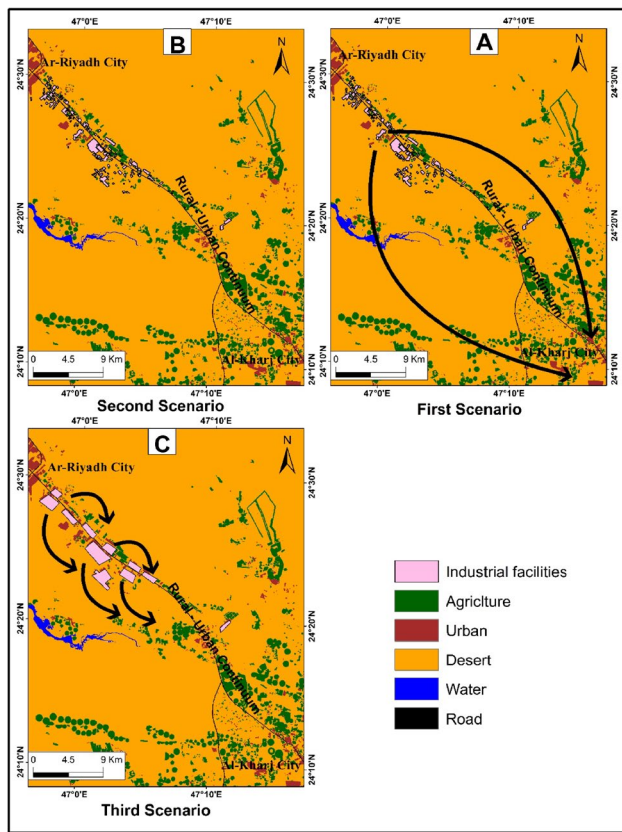
Fig. 14 Scenarios to reduce the increase of the industrial usage control in the map of using the rural–urban–continuum land in 2030

of the entire activities, in addition to the compensation that the responsible authorities would have to pay upon expropriating the lands on which the industrial establishments are located, and it provides job opportunities for the population

and limiting the migration of residents to the two centers (Ar-Riyadh-Al-Kharj).

Conclusions

- The map of land use changes in the urban rural area (Ar-Riyadh-Al-Kharj) during the period between 1988 and 2019 revealed that the lands that were transformed into urban and industrial areas reached 77.84 km^2; it included the largest proportion of these changes from the desert areas, and it included the southern lands Al-Sharqiyah, adjacent to Ar-Riyadh, and northwest adjacent to Al-Kharj, as well as the adjacent lands around the main road network (Ar-Riyadh-Al-Kharj), in addition to the expansions that took place from leveling some agricultural lands. The lands that were transformed into water marshes reached an area of 7.36 km^2. The largest proportion of these changes included the desert areas with increase in the area of Al-Ha'ir sabkha located to the west. As for agricultural lands, they lost about 61.12 km^2 of its area, and the largest percentage of these changes included the desert areas. This is due to the feature of desertification and dredging spread in the northwest of the city of Al-Kharj around the main road (Ar-Riyadh-Al-Kharj), in addition to bulldozing agricultural lands to establish industrial zones. The desert lands lost about 24.08 km^2 of its area, and the largest percentage of these changes included the urban and industrial areas.

- The compatibility between the spatial suitability map and land cover prediction map in 2030 indicates that about 85% of the urban mass is located in the range of very high spatial and high spatial suitability, which indicates an excellent compatibility between spatial suitability and

Table 20 Evaluation of scenarios to reduce the increase of the industrial usage control

Evaluation standards	Scenarios to reduce the increase of the industrial usage control		
	First	Second	Third
Supporting the direction of the national urban strategy by supporting the diversification of the economic base on the axis as a major axis in the central sector	1	2	3
Taking into account the recommendations of the regional plan for Al-Kharj governorate by emptying the axis except for agricultural and recreational activities	3	0	1
The economic cost of implementing the scenario trend	1	3	2
Environmental impacts resulting from the implementation of the scenario	3	1	2
Social gains that are reflected in the area's population	1	2	2
Limiting the migration of residents to the two urban centers, Ar-Riyadh and Al-Kharj	1	2	3
Integration of existing farms with associated industries	0	3	3
Supporting and strengthening the industrial activity on the axis as an existing and productive activity	0	2	3
Total Rating Score	10	15	19

prediction maps, and this confirms the effectiveness of the techniques used to obtain these results.

- To reduce the increased control of industrial uses in the map of land uses for the urban and rural continuum in 2030, the study proposed three different scenarios, one of which deals with the transfer of industrial facilities towards the city of Al-Kharj, and the other confirms the existence of industrial establishments, while the third scenario deals with the transformation of industrial facilities into cells and the exploitation of urban spaces in them, and the study favored the third scenario to reduce the increased control of industrial uses.
- Although the CA–Markov model is able to predict and simulate the future land cover, it has been combined with the GIS-MCA and the AHP method to improve the accuracy of the prediction for the future land cover map produced for the urban rural continuum between Ar-Riyadh and Al-Kharj.

Recommendations

1. The study recommends that the ratio of 70% or higher has to be considered for spatial suitability for future land cover on the urban–rural continuum axis between Ar-Riyadh and Al-Kharj.
2. Allocating the lands located in the rural–urban continuum between Ar-Riyadh and Al-Kharj and determining its land uses to be recreational and tourist uses, with a building ratio of not more than 10% of the land area.
3. Reorganizing the industrial facilities on the rural–urban continuum axis in the form of industrial cells. Each cell includes the licenses donated by official authorities to ensure stopping polluting the environment. It is preferable to link the industrial cells with the source of raw materials and try to reduce the establishments that will be decided to transfer to other authorized industrial regions.
4. Transferring all the industrial establishments that pollute the environment (especially the non-authorized) to the industrial zone in Al-Kharj. Attempting to evaluate the conditions of the non-polluting industrial establishments related to the source of raw material and related to each other in the production cycle. By this way, the random establishments will be transformed into an industrial cell after rehabilitating it and exploiting the urban spaces in it to add other facilities, in accordance with the principles and standards followed in this regard.
5. Creating land uses to achieve the principles of environmental planning science for industrial areas. For example, the use of a "waste warehouse," which is an area within the industrial zone that collects, classifies, and redistributes the waste according to their types, on

the companies that use them as raw materials, whether inside or outside the industrial zone.

6. Environmental sustainability is one of the necessary requirements for balanced development, and this will only be possible through:

   - The preservation of Wadis
   - Environmental rehabilitation and utilization of existing water resources to contribute the maintaining water, food, and housing security
   - Achieve the foundations for sustainable urban development
   - Mitigation of negative environmental impacts by periodic monitoring of the change in land use using the modern technologies such as remote sensing and GIS

7. Approve the amendment of agricultural land uses with special conditions adopted by the municipality to stop the random construction and urban sprawl in agricultural lands.
8. Intensifying the control over the agricultural lands and preventing any division of these lands for residential purposes.
9. Preventing the establishment of workshops, factories, and other commercial warehouses within agricultural lands.
10. The study suggested three different scenarios to reduce the increased control of industrial uses in the map of land uses for the urban and rural continuum in 2030, and the study favored the third scenario to reduce the increased control of industrial uses.

Declarations

Conflict of interest The authors declare no competing interests.

References

Abd El Karim A, Mohsen A (2020) Integrating GIS accessibility and location- allocation models with multicriteria decision analysis for evaluating quality of life in Buraidah City, KSA, MDPI. Sustainability 12:1–29. https://doi.org/10.3390/su12041412 (Accessed on 8/6/2020)

Abdelkarim A (2020) Improving the urban planning of the green zones in Al-Dammam Metropolitan Area, KSA, using integrated GIS location-allocation and accessibility models. Geosfera Indonesia 1:1–46. https://doi.org/10.19184/geosi.v5i1.16708 (Accessed on 8/6/2020)

Abdelkarim A, Al-Alola S, Alogayell H, Mohamed S, Alkadi I, Ismail I (2020) Integration of GIS-based multicriteria decision analysis and analytic hierarchy process to assess flood hazard on the Al-Shamal Train Pathway in Al-Qurayyat Region Kingdom of Saudi Arabia, MDPI. Water 12:1–28. https://doi.org/10.3390/w12061702 (Accessed on 8/6/2020)

Abudeif A, Abdel Moneim A, Farrag A (2015) Multi criteria decision analysis based on analytic hierarchy process in GIS environment for siting nuclear power plant in Egypt. Ann Nucl Energy 75:682–692. https://doi.org/10.1016/j.anucene.2014.09.024 (Accessed on 8/6/2020)

Acheampong RA, Anokye PA (2013) Understanding households' residential location choice in Kumasi's peri-urban settlements and the implications for sustainable urban growth. Res Humanit Soc Sci international knowledge sharing platform 3: 60–70. https://www.iiste.org/Journals/index.php/RHSS/article/view/6317/6631 (Accessed on 8/6/2020)

Ahmadreza E, Mehdi S, Amirreza F (2016) Prediction of urban growth through cellular Automata-Markov chain. Bull Soc Roy Sci Liège 85:824–839

Araya K, Mltiku H, Glrmay G, Muktar M (2018) GIS-based multicriteria model for land suitability evaluation of rainfed teff crop production in degraded semi-arid highlands of Northern Ethiopia. Model Earth Syst Environ 4:1467–1486. https://doi.org/10.1007/s40808-018-0499-9 (Accessed on 8/6/2020)

Baja S, Nesati R, Arif S (2018) Land use and land suitability assessment within the context of spatial planning regulation. IOP Conf Ser: Earth Environ Sci 157:1–7. https://doi.org/10.1088/1755-1315/157/1/012025 (Accessed on 8/6/2020)

Batty M, Xie Y (1994) From cells to cities. Environ Plann B Plann Des 21:531–548. https://doi.org/10.1068/b21S031 (Accessed on 8/6/2020)

Behera MD, Borate SN, Panda SN, Behera PR, Roy PS (2012) Modelling and analyzing the watershed dynamics using Cellular Automata (CA)- Markov model-a geo-information based approach. J Earth Syst Sci 121:1011–1024. https://doi.org/10.1007/s12040-012-0207-5 (Accessed on 8/6/2020)

Carver S (1991) Integrating multi-criteria evaluation with geographical information systems. Int J Geogr Inf Syst 5:321–339. https://doi.org/10.1080/02693799108927858 (Accessedon8/6/2020)

Chakhar S, Mousseau V (2008) GIS-based multicriteria spatial modeling generic framework. Int J Geogr Inf Sci 22:1159–1196. https://doi.org/10.1080/13658810801949827 (Accessed on 8/6/2020)

Congalton RG (1991) A review of assessing the accuracy of classifications of remotely sensed data. Remote Sens Environ 37:35–46. https://doi.org/10.1016/0034-4257(91)90048-B

Dell'Ovo M, Capolongo S, Oppio A (2018) Combining spatial analysis with MCDA for the siting of healthcare facilities. Land Use Policy 76:634–644. https://doi.org/10.1016/j.landusepol.2018.02.044 (Accessed on 8/6/2020)

Ding Y, Zhang Y (2007) The simulation of urban growth aapplying SLEUTH CA model to the Yilan Delta in Taiwan. Jurnal Alam Bina 2007(9):95–107

Feddema JJ, Oleson KW, Bonan GB, Mearns LO, Buja LE, Meehl GA, Washington WM (2005) The importance of land-cover change in simulating future climates. Sci Am Assoc Adv Sci 310:1674–1678. https://doi.org/10.1126/science.1118160 (Accessed on 8/6/2020)

Foley JA, DeFries R, Asner GP, Barford C, Bonan G, Carpenter SR, Chapin FS, Coe MT, Daily GC, Gibbs HK, Joseph H, Holloway T, Howard E, Kucharik C, Monfreda C, Patz J, Prentice C, Ramankutty N, Snyder P (2005) Global consequences of land use. Science 309:570–574. https://doi.org/10.1126/science.1111772 (Accessed on 8/6/2020)

Geist HJ, Lambin EF (2001) What drives tropical deforestation; LUCC Report Series. UCC Int Proj Once 4:1–136

Gibbs HK, Salmon JM (2015) Mapping the world's degraded lands. Appl Geogr Sci Direct 57:12–21. https://doi.org/10.1016/j.apgeog.2014.11.024 (Accessed on 8/6/2020)

Guan DJ, Li HF, Inohae T, Su W, Nagaie T, Hokao K (2011) Modeling urban land use change by the integration of cellular automaton and Markov model. Ecol Model Sci Direct 222:3761–3772. https://doi.org/10.1016/j.ecolmodel.2011.09.009 (Accessed on 8/6/2020)

Hasan Z, Mohsen A, Philip K, Mohammadreza K, Himan S, Anuer A, Mohamed N, Saro L (2019) GIS Multi-criteria analysis by ordered weighted averaging (OWA): toward an integrated citrus management strategy. Sustainability, MDPI 11:1–17. https://doi.org/10.3390/su11041009 (Accessed on 8/6/2020)

He C, Okada N, Zhang Q, Shi P, Li J (2008) Modelling dynamic urban expansion processes incorporating a potential model with cellular automata. Landsc Urban Plan 86:79–91. https://doi.org/10.1016/j.landurbplan.2007.12.010 (Accessed on 8/6/2020)

He J, Huang J, Li C (2017) The evaluation for the impact of land use change on habitat quality: a joint contribution of cellular automata scenario simulation and habitat quality assessment model. Ecol Model Sci Direct 366:58–67. https://doi.org/10.1016/j.ecolmodel.2017.10.001 (Accessed on 8/6/2020)

He J, Huang J, Li C (2017) The evaluation for the impact of land use change on habitat quality: a joint contribution of cellular automata scenario simulation and habitat quality assessment model. Ecol Model 366:58–67. https://doi.org/10.1016/j.ecolmodel.2017.10.001 (Accessed on 8/6/2020)

Hosonuma N, Herold M, De Sy V, De Fries RS, Brockhaus M, Verchot L, Angelsen A, Romijn E (2012) An assessment of deforestation and forest degradation drivers in developing countries. Environ Res Lett 7:1–13. https://doi.org/10.1088/1748-9326/7/4/044009 (Center for International Forestry Research (CIFOR), Bogor, Indonesia (Accessed on 8/6/2020))

Huiping H, Qiangzi L, Yuan Z (2019) Urban residential land suitability analysis combining remote sensing and social sensing data: a case study in Beijing China. Sustainability, MDPI 11:1–19. https://doi.org/10.3390/su11082255 (Accessed on 8/6/2020)

Janssen R, Rietveld P (1990) Multicriteria analysis and geographical information systems: an application to agricultural land use in the Netherlands. In: Scholten, H.J., Stillwell, J.C.H. (eds):

Geographical Information Systems for Urban and Regional Planning. Kluwer, Dordrecht, 17:129–139 https://doi.org/10.1007/978-94-017-1677-2_12. (Accessed on 8/6/2020)

Jin J, Álvaro RA (2017) multicriteria GIS-based assessment to optimize biomass facility sites with parallel environment—a case study in Spain, Energies 10:1–4. https://doi.org/10.3390/en10122095. (Accessed on 8/6/2020)

Kombe WJ (2005) Land use dynamics in peri-urban areas and their implications on the urban growth and form: the case of Dar es Salaam, Tanzania. Habitat Int Sci Direct 29:113–135. https://doi.org/10.1016/S0197-3975(03)00076-6. (Accessed on 8/6/2020)

Lee M, Yeh C (2009) Applying remote sensing techniques to monitor shifting wetland vegetation: a case study of Danshui River estuary mangrove communities Taiwan. Ecol Eng 35:487–496. https://doi.org/10.1016/j.ecoleng.2008.01.007 (Accessed on 8/6/2020)

Li X, Chen Y, Liu X, Xu X, Chen G (2017) Experiences and issues of using cellular automata for assisting urban and regional planning in China. Int J Geogr Inf Sci 31:1606–1629. https://doi.org/10.1080/13658816.2017.1301457 (Accessed on 8/6/2020)

Liu Y (2009) Modelling urban development with geographical information system and celluar atutomata Boca Raton, FL: Taylor and Francis Group 1–186 https://doi.org/10.1201/9781420059908 (Accessed on 8/6/2020).

Liu X, Liang X, Li X, Xu X, Ou J, Chen Y, Li S, Wang S, Pei F (2017) A future land use simulation model (FLUS) for simulating multiple land use scenarios by coupling human and natural effects. Landsc Urban Plan 168:94–116. https://doi.org/10.1016/j.landurbplan.2017.09.019 (Accessed on 8/6/2020)

Malczewski J (1999) GIS and multi-criteria decision analysis. Wiley, New York, 1–408. https://www.wiley.com/en-us/GIS+and+Multicriteria+Decision+Analysis-p-9780471329442. (Accessed on 8/6/2020)

Malczewski J (2006) GIS-based multi-criteria decision analysis: a survey of the literature. Int J Geogr Inf Sci 20:703–726. https://doi.org/10.1080/13658810600661508 (Accessed on 8/6/2020)

Mandere MN, Ness B, Anderberg S (2010) Peri-urban development, livelihood change and household income: a case study of peri-urban Nyahururu, Kenya. J. Agric. Ext. Rural Dev. Academic Journal, Lagos, Nigeria 2, 73–83. https://academicjournals.org/journal/JAERD/article-full-text-pdf/25A60595890 (Accessed on 8/6/2020)

Mbiba B, Huchzermeyer M (2002) Contentious development: peri-urban studies in sub-Saharan Africa. Prog Dev Stud Sega J 2:113–131. https://doi.org/10.1191/2F1464993402ps032ra (Accessed on 8/6/2020)

Merlos F, Monzon P, Mercau L, Taboada M, Andrade H, Hall J, Jobbagy E, Cassman G, Grassini P (2015) Potential for crop production increase in argentina through closure of existing yield gaps. Field Crop Res 184:145–154. https://doi.org/10.1016/j.fcr.2015.10.001 (Accessed on 8/6/2020)

Mubea K, Goetzke R, Menz G (2014) Applying cellular automata for simulating and assessing urban growth scenario based in Nairobi Kenya. Int J Adv Comput Sci Appl 5:1–13. https://doi.org/10.14569/IJACSA.2014.050201 (The science and information organization, West Yorkshire, United Kingdom (Accessed on 8/6/2020))

Mwangi H, Lariu P, Julich S, Patil S, McDonald M, Feger K (2017) Characterizing the intensity and dynamics of land-use change in the Mara River Basin, East Africa. Forests, MDPI, Basel, Switzerland 9:8. https://doi.org/10.3390/f9010008 (Accessed on 8/6/2020)

Oguz H, Klein AG, Srinivasan R (2007) Using the sleuth urban growth model to simulate the impacts of future policy scenarios on urban land use in the Houston-Galveston-Brazoria CMSA. Res J Soc Sci 2:72–82

Pakawan C, Saowanee W (2019) Predicting urban expansion and urban land use changes in Nakhon Ratchasima City using a CA-Markov Model under two different scenarios. Land, MPDI 8:1–16. https://doi.org/10.3390/land8090140 (Accessed on 8/6/2020)

Pan G, Pan J (2012) Research in cropland suitability analysis based on GIS. Inter Confer Comput Comput Technol Agric 365:314–325. https://doi.org/10.1007/978-3-642-27278-3_33 (Accessed on 8/6/2020)

Parsa VA, Salehi E (2016) Spatio-temporal analysis and simulation pattern of land use/cover changes, case study: Naghadeh. Iran J Urban Manage 5:43–51. https://doi.org/10.1016/j.jum.2016.11.001 (Accessed on 8/6/2020)

Rahel H, Heiko B, Kamal K (2018) Predicting land use/land cover changes using a CA-Markov model under two different scenarios. MDPI, Sustainability 10:1–23. https://doi.org/10.3390/su10103421. (Accessed on 8/6/2020)

Reynolds K, Hessburg P (2014) An overview of the ecosystem management decision-support system. In: Reynolds KM, Hessburg PF, Bourgeron PS (Eds) Making transparent environmental management decisions. Springer, Berlin, 3–22. https://doi.org/10.1007/978-3-642-32000-2_1. (Accessed on 8/6/2020)

Rinner C, Heppleston A (2006) The spatial dimensions of multi-criteria evaluation–case study of a home buyer's spatial decision support system. Int Conf Geogr Inf Sci 4197:338–352. https://doi.org/10.1007/11863939_22 (Accessed on 8/6/2020)

Saaty T (1980) The analytic hierarchy process. McGraw-Hill, New York

Saidi S, Hosni H, Mannai F, Jelassi S, Bouri B (2017) Anselme, GIS-based multi-criteria analysis and vulnerability method for the potential groundwater recharge delineation, case study of Manouba phreatic aquifer, NE Tunisia. Environ Earth Sci 76:511. https://doi.org/10.1007/s12665-017-6840-1 (Accessed on 8/6/2020)

Santé I, Garcia AM, Miranda D, Crecente R (2010) Cellular automata models for the simulation of real-world urban processes: a review and analysis. Landsc Urban Plan Sci Direct 96:108–122. https://doi.org/10.1016/j.landurbplan.2010.03.001 (Accessed on 8/6/2020)

Silva EA, Clarke KC (2002) Calibration of the SLEUTH urban growth model for Lisbon and Porto, Portugal. Comput Environ Urban Syst 26:525–552. https://doi.org/10.1016/S0198-9715(01)00014-X (Accessed on 8/6/2020)

Simon H (1977) The logic of heuristic decision making. In: Models of Discovery. Boston Studies in the Philosophy of Science, Springer, Dordrecht 54:154–172 https://link.springer.com/chapter/10.1007%2F978-94-010-9521-1_10. (Accessed on 8/6/2020)

Simon D, Mcgregor D, Nsiah-Gyabaah K (2004) The changing urban-rural interface of African cities: definitional issues and an application to Kumasi. Ghana Environ Urban Sega J 16:235–248. https://doi.org/10.1177/2F095624780401600214. (Accessed on 8/6/2020)

Solomon H, Woldeamlak B, Jan N, James L (2019) Analysing past land use land cover change and CA-Markov-based future modelling in the Middle Suluh Valley, Northern Ethiopia, Geocarto International 35:1–32. https://doi.org/10.1080/10106049.2018.1516241. (Accessed on 8/6/2020)

Taher O, David S, Emad K (2018) An integrated land use change model to simulate and predict the future of greater Cairo metropolitan region. J Land Use Sci 13:565–584. https://doi.org/10.1080/1747423X.2019.1581849 (Accessed on 8/6/2020)

Tajbakhsh M, Memarian H, Shahrokhi H (2016) Analyzing and modeling urban sprawl and land use changes in a developing city using a CA-Markovian approach. Glob J Environ Sci Manag Iran 2:397–410. https://doi.org/10.22034/gjesm.2016.02.04.009 (Accessed on 8/6/2020)

Thuo ADM (2010) Community and social responses to land use transformations in the Nairobi Rural-Urban Fringe, Kenya. Field Actions Science Reports, Paris, 1:1–11 https://journals.opene dition.org/factsreports/435 (Accessed on 8/6/2020)

Turner BL (1994) II. Local faces, global flows: the role of land use and land cover in global environmental change. Land Degrad Rehabil 5:71–78. https://doi.org/10.1002/ldr.3400050204 (Accessed on 8/6/2020)

Tzeng G, Huang J (2011) Multiple attribute decision making: methods and applications, Chapman and Hall/CRC 1st edition, 1–352

Van den Bossche J, De Baets B, Verwaeren J, Botteldooren D, Theunis J (2018) Development and evaluation of land use regression models for black carbon based on bicycle and pedestrian measurements in the urban environment. Environ Model Softw 99:58–69. https://doi.org/10.1016/j.envsoft.2017.09.019 (Accessed on 8/6/2020)

Webster C, Wu F (2001) Coase, spatial pricing and self-organizing cities. Urban Stud 38:2037–2054. https://doi.org/10.1080/2F004 20980120080925 (Accessed on 8/6/2020)

White R, Engelen G (1994) Cellular dynamics and GIS: modelling spatial complexity. Geogr Syst 1994(1):237–253

White R, Engelen G (2000) High-resolution integrated modelling of the spatial dynamics of urban and regional systems computers. Comput Environ Urban Syst Sci Direct 24:383–400. https://doi.org/10.1016/S0198-9715(00)00012-0 (Accessed on 8/6/2020)

White R, Engelen V (2000) High resolution integrated modeling of the spatial dynamics of urban and regional systems. Comput Environ Urban Syst 24:383–400. https://doi.org/10.1016/S0198-9715(00)00012-0 (Accessed on 8/6/2020)

Wu F (1998) SimLand: a prototype to simulate land conversion through the integrated GIS and CA with AHP-derived transition rules. Int J Geogr Inf Sci 12:63–82. https://doi.org/10.1080/1365881982 42012 (Accessed on 8/6/2020)

Wu F (2002) Calibration of stochastic cellular automata: the application to rural–urban land conversions. Int J Geogr Inf Sci 16:795–818. https://doi.org/10.1080/13658810210157769 (Accessed on 8/6/2020)

Xu X, Du Z, Zhang H (2016) Integrating the system dynamic and cellular automata models to predict land use and land cover change. Int J Appl Earth Obs Geoinf 52:568–579. https://doi.org/10.1016/j.jag.2016.07.022 (Accessed on 8/6/2020)

Yatsalo B, Didenko V, Tkachuk A, Gritsyuk G, Mirzeabasov O, Slipenkaya V, Babutski A, Pichugina I, Sullivan T, Linkov I (2010) Multi-criteria spatial decision support system DECERNS: Application to land use planning, International Journal of Information Systems and Social Change, 1:11–30 https://www.igi-global.com/gateway/article/38993 (Accessed on 8/6/2020)

Zadbagher E, Becek K (2018) Modeling land use/land cover change using remote sensing and geographic information systems: case study of the Seyhan. Environ Monit Assess 190:494. https://doi.org/10.1007/s10661-018-6877-y